A posteriori stopping criteria for space-time domain decomposition for the heat equation in mixed formulations

Sarah Ali Hassan, Caroline Japhet, Martin Vohralík

▶ **To cite this version:**

A posteriori stopping criteria for space-time domain decomposition for the heat equation in mixed formulations[*]

Sarah Ali Hassan[†], Caroline Japhet[‡] and Martin Vohralík[†]

June 14, 2018

Abstract

We propose and analyse a posteriori estimates for global-in-time, nonoverlapping domain decomposition methods for heterogeneous and anisotropic porous media diffusion problems. We consider mixed formulations, with a lowest-order Raviart–Thomas–Nédélec discretization, often used for such problems. Optimized Robin transmission conditions are employed on the space-time interface between subdomains, and different time grids are used to adapt to different time scales in the subdomains. Our estimators allow to distinguish the spatial discretization, the temporal discretization, and the domain decomposition error components. We design an adaptive space-time domain decomposition algorithm, wherein the iterations are stopped when the domain decomposition error does not affect significantly the global error. Overall, a guaranteed bound on the overall error is obtained on each iteration of the space-time domain decomposition algorithm, and simultaneously important savings in terms of the number of domain decomposition iterations can be achieved. Numerical results for two-dimensional problems with strong heterogeneities and local time stepping are presented to illustrate the performance of our adaptive domain decomposition algorithm.

Key words: Mixed finite element method, global-in-time domain decomposition, nonconforming time grids, Robin interface conditions, a posteriori error estimate, stopping criteria

1 Introduction

In many simulations of time-dependent physical phenomena, such as flow and transport in porous media, the domain of calculation is a union of subdomains with different physical properties, in which the time scales may be very different. In this article we are concerned with space-time domain decomposition algorithms, well-suited to non-matching time grids, for solving the following diffusion problem with final time $T > 0$: find the potential p and the flux $\mathbf{u}$ such that:

$$\mathbf{u} = -\boldsymbol{S}\nabla p \quad \text{in} \quad \Omega \times (0, T), \tag{1.1a}$$

$$\frac{\partial p}{\partial t} + \nabla \cdot \mathbf{u} = f \quad \text{in} \quad \Omega \times (0, T), \tag{1.1b}$$

$$p = g_{\mathrm{D}} \quad \text{on} \quad \Gamma^{\mathrm{D}} \times (0, T), \tag{1.1c}$$

$$-\mathbf{u} \cdot \mathbf{n} = g_{\mathrm{N}} \quad \text{on} \quad \Gamma^{\mathrm{N}} \times (0, T), \tag{1.1d}$$

$$p(\cdot, 0) = p_0 \quad \text{in} \quad \Omega, \tag{1.1e}$$

where $\Omega \subset \mathbb{R}^d$, $d = 2, 3$, is a polygonal (polyhedral if $d = 3$) domain (open, bounded and connected set) with Lipschitz-continuous boundary $\partial\Omega$ decomposed into two connected sets Γ^{D} and Γ^{N} with Γ^{D} of

[†]Inria Paris, 2 rue Simone Iff, 75589 Paris, France & Université Paris-Est, CERMICS (ENPC), 77455 Marne-la-Vallée 2, France `sarah.ali-hassan@inria.fr, martin.vohralik@inria.fr`.

[‡]Université Paris 13, Sorbonne Paris Cité, LAGA, CNRS (UMR 7539), 93430, Villetaneuse, France `japhet@math.univ-paris13.fr`.

nonzero $(d-1)$-dimensional measure, $g_{\mathrm{N}} \in L^2(\Gamma^{\mathrm{N}} \times (0,T))$ is the Neumann boundary condition, $g_{\mathrm{D}} \in H^{\frac{1}{2}}(\Gamma^{\mathrm{D}} \times (0,T)) \cap C^0((\overline{\Gamma}^{\mathrm{D}}) \times (0,T))$ is the Dirichlet boundary condition, and $p_0 \in H^1(\Omega)$ is the initial condition with $p_0|_{\Gamma^{\mathrm{D}}} = g_{\mathrm{D}}(\cdot,0)|_{\Gamma^{\mathrm{D}}}$. Furthermore, $f \in L^2(\Omega \times (0,T))$ is the source term, $\mathbf{n}$ is the outward unit normal vector to $\partial\Omega$, and $\boldsymbol{S}$ is a symmetric, bounded, and uniformly positive definite tensor whose terms are for simplicity supposed piecewise constant on the mesh $\mathcal{T}_h$ of Ω defined below and constant in time. We consider global-in-time optimized Schwarz method which uses the optimized Schwarz waveform relaxation (OSWR) approach [31, 49]. This is an iterative method that computes in the subdomains over the whole space-time interval, exchanging space-time boundary data through transmission conditions on the space-time interfaces. The OSWR algorithm uses more general (Robin or Ventcell) transmission operators in which coefficients can be optimized to improve convergence rates, see [31, 42, 49]. The optimization of the Robin (or Ventcell) parameters was analyzed in [10, 12]. Generalizations to heterogeneous problems with nonmatching time grids were introduced in [11, 13, 30, 34, 35, 36, 37, 41, 40, 39]. More precisely, in [13, 36, 37], a discontinuous Galerkin (DG) method for the time discretization of the OSWR algorithm was introduced and analyzed for the case of nonconforming time grids. A suitable time projection between subdomains is defined using an optimal projection algorithm as in [33, 32] with no additional grid. In the context of mixed finite elements, which are mass conservative and handle well heterogeneous and anisotropic diffusion tensors, we refer also to [23, 41, 39]. The multi-domain problem can actually be reformulated as an interface problem (see [21], [39], or [3]) that can be solved by various iterative methods, such as block-Jacobi or GMRES.

Our first objective in this contribution is to design a posteriori estimates valid on each step of the space-time domain decomposition algorithm. For general algebraic iterative solvers, several techniques with residual-based estimates have been developed, see [9, 6, 7], see also [53, 50, 57] for goal-oriented a posteriori error estimates. A general framework for any numerical method and any algebraic solver has been introduced in [26], building on the ideas from [43], and has been extended to coupled unsteady nonlinear and degenerate problems in [15, 20]. For lowest-order time discretizations, this approach is based on a $H^1(\Omega)$-conforming reconstruction of the potential, continuous and piecewise affine in time, and an equilibrated $\mathbf{H}(\mathrm{div},\Omega)$-conforming reconstruction of the flux, piecewise constant in time. It yields a guaranteed and fully computable upper bound on the error measured in the energy norm augmented by a dual norm of the time derivative (see [61, 25]), without unknown constants. Using a globally equivalent norm, which contains also the temporal jumps of the numerical solution, it leads to local space-time efficiency, see the recent contribution [24].

Recently, a posteriori error estimates and stopping criteria for non-overlapping domain decomposition algorithms such as FETI [28] or BDD [48, 17], have been proposed in [58, 59]. Both upper and lower bounds for the overall error are derived, and the discretization and the domain decomposition error components are distinguished. Also this approach is based on $H^1(\Omega)$-conforming potential and $\mathbf{H}(\mathrm{div},\Omega)$-conforming flux reconstructions, and follows the a posteriori techniques of [55, 46, 56, 27]. A key observation is that such reconstructions can be easily obtained when the solution approach involves subdomain problems with both Dirichlet and Neumann interface conditions on each domain decomposition (DD) iteration, as this is the case for FETI or BDD.

For domain decomposition strategies with more general interface conditions, and where neither the conformity of the flux nor that of the potential is preserved (as long as the convergence is not reached), a new adaptive domain decomposition algorithm has been introduced in [3]. More precisely, three reconstructions are proposed: a flux reconstruction that is globally $\mathbf{H}(\mathrm{div},\Omega)$-conforming and locally conservative in each mesh element, based on the construction of [54, Section 3.5.2], as well as two H^1-conforming potential reconstructions, one globally on Ω, relying on the averaging operator $\mathcal{I}_{\mathrm{av}}$, see [1, 44, 14], and another on each subdomain Ω_i, which introduces weights on the interfaces and whose goal is to separate the DD and the discretization components. Then, error control is achieved on each step and an adaptive domain decomposition algorithm is proposed wherein the iterations are stopped when the domain decomposition error does not affect significantly the overall error.

This paper is a continuation of [3]: we provide a new approach that makes it possible to extend this adaptive domain decomposition algorithm to model coupled time-dependent diffusion problems. We focus on mixed finite element discretizations in the subdomains and extend the approaches from [45, 62, 2, 63, 54, 25, 24, 3] for a posteriori error estimates. We first build a flux reconstruction that is globally $\mathbf{H}(\mathrm{div},\Omega)$-conforming, locally conservative in each mesh element, and piecewise constant in time. Following [3], a

simple coarse balancing problem is first solved, and then we solve a local Neumann problem in a band around the interfaces in each subdomain by the mixed finite element method. Finally, two H^1-conforming potential reconstructions are built. One is standard relying on the adjustement of the averaging operator $\mathcal{I}_{\text{av}}$ for parabolic problems following [25], whereas the other one uses weights on the interfaces following [3] to separate the space-time DD and the discretization components.

The outline of this paper is as follows: after introducing some useful notations in Section 2, we present in Section 3 the multi-domain formulation using the global-in-time optimized Schwarz method and reformulate it as a space-time interface problem. We next detail the fully discrete interface problem using the mixed finite element method in space and the discontinuous Galerkin method of order zero in time. This interface problem can be solved using either a block-Jacobi or a GMRES method. In Section 4, we derive a fully computable upper bound for the error between the exact and the approximate numerical solution on a given DD iteration, in the energy norm. The details about the employed flux and potential reconstructions are given in Section 5. Finally, in Section 6, we show numerical results for a two-dimensional problem with strong heterogeneities, inspired from a problem which simulates the transport of contaminant in and around a nuclear waste repository site. It relies on the GMRES iterations and testifies tight overall error control, simultaneously for the error due to the domain decomposition and nonconforming time grids, and important reduction of the number of space-time DD iterations.

2 Preliminaries

In this section we introduce the partition of the domain Ω and some function spaces following the same notations given in [3].

2.1 Partitions of the domain Ω

We suppose that the domain Ω is decomposed into $\mathcal{N}$ non-overlapping polygonal subdomains Ω_i, $i \in [\![1, \mathcal{N}]\!]$, such that $\overline{\Omega} = \bigcup\limits_{i=1}^{\mathcal{N}} \overline{\Omega}_i$. For all $i \in [\![1, \mathcal{N}]\!]$, let $\Gamma_i^{\text{N}} := \Gamma^{\text{N}} \cap \partial\Omega_i$, $\Gamma_i^{\text{D}} := \Gamma^{\text{D}} \cap \partial\Omega_i$, and $\mathbf{n}_i$ be the unit outward-pointing normal of $\partial\Omega_i$. Let B^i be the set of neighbors of the subdomain Ω_i that share at least one edge if $d = 2$ with Ω_i (face if $d = 3$) and let $|B^i|$ be the cardinality of this set. Using this notation, we introduce the interface $\Gamma_{i,j} := \partial\Omega_i \cap \partial\Omega_j$, $j \in B^i$, between two adjacent subdomains Ω_i and Ω_j. Consequently, $\partial\Omega_i = \Gamma_i^{\text{N}} \cup \Gamma_i^{\text{D}} \cup \Gamma_i$ with $\Gamma_i := \bigcup\limits_{j \in B^i} \Gamma_{i,j}$. We also define $\Gamma := \bigcup\limits_{i \in [\![1,\mathcal{N}]\!]} \Gamma_i$.

We then define $\mathcal{T}_h := \bigcup\limits_{i=1}^{\mathcal{N}} \mathcal{T}_{h,i}$, where $\mathcal{T}_{h,i}$ is a regular triangulation of the subdomain Ω_i, such that $\overline{\Omega}_i = \bigcup\limits_{K \in \mathcal{T}_{h,i}} K$, where $|\mathcal{T}_{h,i}|$ is the number of triangles (tetrahedra if d=3) in the i-th subdomain. We suppose that $\mathcal{T}_{h,i}$ is a conforming mesh, i.e., such that if $K, K' \in \mathcal{T}_{h,i}$, $K \neq K'$, then $K \cap K'$ is either an empty set or a common vertex or edge or face. For simplicity, we also assume that $\mathcal{T}_h$ is conforming, although this assumption could be easily avoided by introducing the concept of a simplicial submesh as in, e.g., [54, 22] and the references therein. We denote the set of all edges (faces if $d = 3$) of $\mathcal{T}_{h,i}$ by $\mathcal{E}_{h,i}$, and the set of all edges (faces) of $K \in \mathcal{T}_h$ by $\mathcal{E}_K$. $\mathcal{E}_{h,i}^{\text{int}}$ is the set of interior edges (faces) of the subdomain Ω_i, $\mathcal{E}_{h,i}^{\text{ext}} := \mathcal{E}_{h,i}^{\Gamma_{\text{D}}} \cup \mathcal{E}_{h,i}^{\Gamma_{\text{N}}}$ is the set of boundary edges (faces) on $\partial\Omega \cap \partial\Omega_i$, and $\mathcal{E}_h^{\Gamma_{i,j}}$ is the set of edges (faces) on the interface $\Gamma_{i,j}$. Then $\mathcal{E}_{h,i} = (\bigcup\limits_{j \in B^i} \mathcal{E}_h^{\Gamma_{i,j}}) \cup \mathcal{E}_{h,i}^{\text{int}} \cup \mathcal{E}_{h,i}^{\text{ext}}$. Let h_K denote the diameter of K and let h_i be the largest diameter of all triangles (tetrahedra if $d = 3$) in $\mathcal{T}_{h,i}$, i.e., $h_i := \max\limits_{K \in \mathcal{T}_{h,i}} h_K$.

2.2 Partitions of the time interval $(0, T)$

For $i \in [\![1, \mathcal{N}]\!]$, let $\{t^{n,i}\}_{0 \le n \le N_i}$ be a sequence of discrete times of the subdomain Ω_i with $t^{0,i} = 0 < t^{1,i} < \cdots < t^{N_i-1,i} < t^{N_i,i} = T$. We denote by $\mathcal{T}_{\tau,i}$ the partition of the time interval $(0, T)$ into subintervals $I_{n,i} := (t^{n-1,i}, t^{n,i}]$ and set $\tau^{n,i} := t^{n,i} - t^{n-1,i}$ for all $1 \le n \le N_i$. The partition $\mathcal{T}_{\tau,i}$ of Ω_i is possibly different from the partition $\mathcal{T}_{\tau,j}$ of the neighboring subdomain Ω_j, $j \in B^i$. Though our space-time DD supports such nonconforming time grids, in our a posteriori error analysis, we will additionally need an intersection of all the different time meshes (coarsest common refinement of all individual time grids):
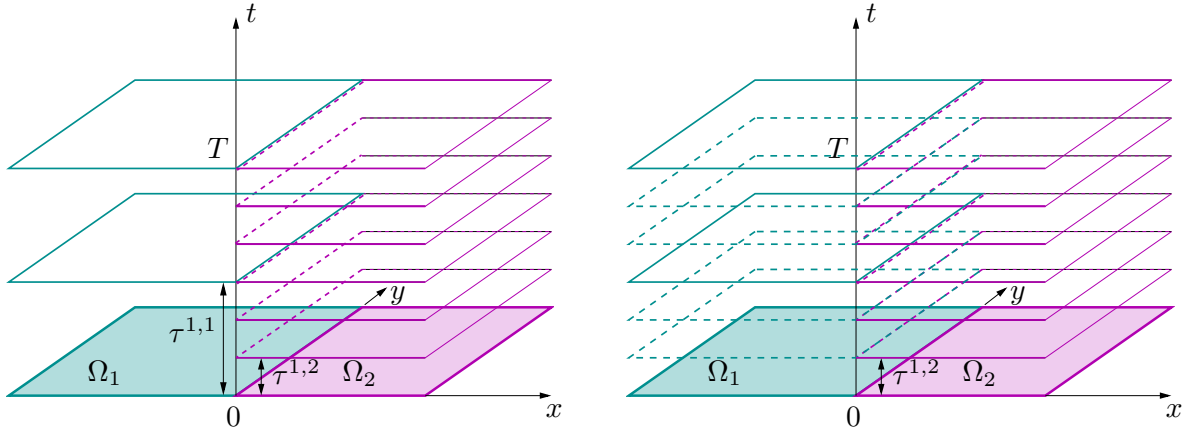
Figure 1: Nonconforming time grids between two subdomains Ω_1 and Ω_2 (left) and the intersection time grid (right)

$\mathcal{T}_\tau := \{t^n\}_{0 \leq n \leq N} = \bigcup\limits_{i=1}^{\mathcal{N}} \{t^{n,i}\}_{0 \leq n \leq N_i}$, with $I_n := (t^{n-1}, t^n]$ and $\tau^n := t^n - t^{n-1}$ for all $1 \leq n \leq N$. An illustration is given in Figure 1, for the case of two subdomains. Practically, the most appropriate case is when the time grids in the individual subdomains are not completely independent but rather stem from subrefinement of some common time grid.

2.3   Some functions spaces

We recall here the definition of some basic function spaces. For a given non-empty domain $D \subset \Omega$ and a real number l, $1 \leq l \leq \infty$, we employ the standard functional notations $L^l(D)$ and $\mathbf{L}^l(D) := [L^l(D)]^d$ of Lebesgue spaces. We denote by $(\cdot, \cdot)_D$ the scalar product for $L^2(D)$ and $\mathbf{L}^2(D)$, associated with the norm $\|\cdot\|_D$, and by $|D|$ the Lebesgue measure of D. Shall $D = \Omega$, the index will be dropped. Let $\langle \cdot, \cdot \rangle_\gamma$ be the scalar product for the $d-1$ dimensional $L^2(\gamma)$ on $\gamma = \partial D$ or a subset of it. Let also $H^1(D) := \{v \in L^2(D); \nabla v \in \mathbf{L}^2(D)\}$ be the Sobolev space of scalar-valued functions with weak derivatives square-integrable and let $\mathbf{H}(\text{div}, D) := \{\mathbf{v} \in \mathbf{L}^2(D); \nabla \cdot \mathbf{v} \in L^2(D)\}$ be the space of vector-valued functions whose weak divergences are square-integrable. Finally, for any scalar-, vector-, or tensor-valued function φ defined on Ω, we let φ_i denote the restriction of φ to Ω_i, $i = 1, .., \mathcal{N}$.

3   The global-in-time optimized Schwarz method using OSWR

In this section we describe a nonoverlapping space-time domain decomposition method using optimized Schwarz waveform relaxation (OSWR) [10, 12, 31, 49], in the context of a mixed formulation, see [39, 41]. This method is global in time and allows to use different time steps in different subdomains, see [11, 13, 30, 34, 35, 36, 37, 39, 41]. The time projection between subdomains is obtained by a projection algorithm with linear complexity and without any additional grid, see [32, 33]. Using the notations of Section 2, the original problem (1.1) can be reformulated as the following equivalent multi-domain problem, for $i \in [\![1, \mathcal{N}]\!]$:

$$\mathbf{u}_i = -\boldsymbol{S} \nabla p_i \quad \text{in} \quad \Omega_i \times (0, T), \tag{3.1a}$$

$$\frac{\partial p_i}{\partial t} + \nabla \cdot \mathbf{u}_i = f \quad \text{in} \quad \Omega_i \times (0, T), \tag{3.1b}$$

$$p_i = g_{\mathrm{D}} \quad \text{on} \quad \Gamma_i^{\mathrm{D}} \times (0, T), \tag{3.1c}$$

$$-\mathbf{u}_i \cdot \mathbf{n} = g_{\mathrm{N}} \quad \text{on} \quad \Gamma_i^{\mathrm{N}} \times (0, T), \tag{3.1d}$$

$$p(\cdot, 0) = p_0(\cdot) \quad \text{in} \quad \Omega_i, \tag{3.1e}$$

together with the "natural" transmission conditions on the space-time interfaces:

$$p_i = p_j \quad \text{and} \quad \mathbf{u}_i \cdot \mathbf{n}_i + \mathbf{u}_j \cdot \mathbf{n}_j = 0 \quad \text{on} \quad \Gamma_{i,j} \times (0,T), \ \forall j \in B^i, \tag{3.2}$$

which ensure the continuity of the potential p and of the normal trace of the flux $\mathbf{u}$ on the interface $\Gamma_{i,j} \times (0,T)$. Alternatively, one may replace the natural conditions (3.2) by equivalent Robin transmission conditions [47] as follows

$$-\beta_{i,j}\mathbf{u}_i \cdot \mathbf{n}_i + p_i = -\beta_{i,j}\mathbf{u}_j \cdot \mathbf{n}_i + p_j \quad \text{on} \quad \Gamma_{i,j} \times (0,T), \ \forall j \in B^i, \tag{3.3}$$

where $\beta_{i,j} > 0$, $j \in B^i$, $i \in [\![1, \mathcal{N}]\!]$ are free parameters that may be optimized to improve the convergence factor of the iterative domain decomposition algorithm, see [10, 29, 31, 42, 49].

As noticed in [39, 3], in the context of mixed finite elements, the potential p_i is in $L^2(\Omega_i)$, so that $p_i|_{\Gamma_{i,j}}$ is not well defined. Thus a Robin condition $-\beta_{i,j}\mathbf{u}_i \cdot \mathbf{n}_i + p_i = \xi_{i,j}$, with a given Robin boundary data $\xi_{i,j}$ on $\Gamma_{i,j} \times (0,T)$ will help to define p_i on $\Gamma_{i,j} \times (0,T)$ through the well-defined expression

$$p_i|_{\Gamma_{i,j}} := \xi_{i,j} + \beta_{i,j}\mathbf{u}_i \cdot \mathbf{n}_i, \tag{3.4}$$

provided that $\mathbf{u}_i \cdot \mathbf{n}_i \in L^2(\Gamma_{i,j})$.

3.1 The continuous space-time interface problem

Using a global-in-time Robin-to-Robin interface operator, the multi-domain problem (3.1) with (3.3) can be reformulated as a problem where the unknowns are located only on the space-time interfaces, see e.g. [3, 18, 34, 39]. We first introduce the following notations, for $i \in [\![1, \mathcal{N}]\!]$,

$$L_T(\Gamma_i) := \prod_{j \in B^i} L^2(0,T; L^2(\Gamma_{i,j})),$$

$$\boldsymbol{\mathcal{V}}_{T,i} := L^2(0,T; L^2(\Omega_i)) \times L^2(0,T; L^2(\Gamma_i^{\mathrm{D}})) \times L^2(0,T; L^2(\Gamma_i^{\mathrm{N}})) \times H^1(\Omega_i).$$

Following [39, 3] and for abstract formulation of the interface problem, we introduce the space $\mathbf{W}_i := \{\mathbf{v} \in \mathbf{H}(\mathrm{div}, \Omega_i); \mathbf{v} \cdot \mathbf{n}_i \in L^2(\partial \Omega_i)\}$ with an increased normal trace regularity to handle Robin conditions. One could possibly weaken this requirement by using the techniques of [16]; in any case, the present a posteriori error analysis does not rely on it. We then define the space $\mathbf{W}_i^{g_{\mathrm{N}}} := \{\mathbf{v} \in \mathbf{W}_i; \mathbf{v} \cdot \mathbf{n}_i = g_{\mathrm{N}} \text{ on } \Gamma^{\mathrm{N}} \cap \partial \Omega_i\}$ of functions verifying the Neumann boundary condition on Γ^{N}. We now introduce the subproblem solution operator for the subdomain Ω_i, $i \in [\![1, \mathcal{N}]\!]$, that maps the available Robin condition $\boldsymbol{\xi}_i$ and equation data stored in the vector $\boldsymbol{\mathcal{F}}_i$ to $\boldsymbol{\xi}_i$ together with the subdomain potential p_i and flux $\mathbf{u}_i$:

$$\mathcal{M}_i : \begin{array}{ccc} L_T(\Gamma_i) \times \boldsymbol{\mathcal{V}}_{T,i} & \to & L_T(\Gamma_i) \times H^1(0,T; L^2(\Omega_i)) \times L^2(0,T; \mathbf{W}_i^{g_{\mathrm{N}}}), \\ (\boldsymbol{\xi}_i, \boldsymbol{\mathcal{F}}_i) & \to & (\boldsymbol{\xi}_i, p_i, \mathbf{u}_i), \end{array} \tag{3.5}$$

where $\boldsymbol{\xi}_i := (\xi_{i,j})_{j \in B^i}$, $\boldsymbol{\mathcal{F}}_i := (f|_{\Omega_i}, g_{\mathrm{D}}|_{\Gamma_i^{\mathrm{D}}}, g_{\mathrm{N}}|_{\Gamma_i^{\mathrm{N}}}, p_0|_{\Omega_i})$, and where $(p_i, \mathbf{u}_i)$ is the solution of the following problem in Ω_i (in an appropriate mixed formulation):

$$\mathbf{u}_i = -\boldsymbol{S}\nabla p_i \quad \text{in} \quad \Omega_i \times (0,T), \tag{3.6a}$$

$$\frac{\partial p_i}{\partial t} + \nabla \cdot \mathbf{u}_i = f \quad \text{in} \quad \Omega_i \times (0,T), \tag{3.6b}$$

$$p_i = g_{\mathrm{D}} \quad \text{on} \quad \Gamma_i^{\mathrm{D}} \times (0,T), \tag{3.6c}$$

$$-\mathbf{u}_i \cdot \mathbf{n}_i = g_{\mathrm{N}} \quad \text{on} \quad \Gamma_i^{\mathrm{N}} \times (0,T), \tag{3.6d}$$

$$-\beta_{i,j}\mathbf{u}_i \cdot \mathbf{n}_i + p_i = \xi_{i,j} \quad \text{on} \quad \Gamma_{i,j} \times (0,T), \ \forall j \in B^i. \tag{3.6e}$$

$$p_i(\cdot, 0) = p_0(\cdot) \quad \text{in} \quad \Omega_i. \tag{3.6f}$$

Using (3.4), we also introduce the operator $\mathcal{R}_i$ that maps the available Robin condition $\boldsymbol{\xi}_i$ together with a potential p_i and flux $\mathbf{u}_i$ to a new Robin datum, $\mathcal{R}_i :$

$$\begin{array}{ccc} L_T(\Gamma_i) \times H^1(0,T; L^2(\Omega_i)) \times L^2(0,T; \mathbf{W}_i^{g_{\mathrm{N}}}) & \to & L_T(\Gamma_i), \\ (\boldsymbol{\xi}_i, p_i, \mathbf{u}_i) & \to & \left(\beta_{j,i}\mathbf{u}_i \cdot \mathbf{n}_i + (\xi_{i,j} + \beta_{i,j}\mathbf{u}_i \cdot \mathbf{n}_i) \right)_{j \in B^i}. \end{array} \tag{3.7}$$

The Robin-to-Robin operator is then defined as:

$$\mathcal{S}_i^{\mathrm{RtR}} := \mathcal{R}_i \circ \mathcal{M}_i : \ L_T(\Gamma_i) \times \boldsymbol{\mathcal{V}}_{T,i} \ \rightarrow \ L_T(\Gamma_i). \tag{3.8}$$

Then condition (3.3) with $(p_i, \mathbf{u}_i)$ solution of the subproblem (3.6) lead to the equivalent space-time interface problem: find $\boldsymbol{\xi} := (\boldsymbol{\xi}_1, \ldots, \boldsymbol{\xi}_{\mathcal{N}}) \in L_T(\Gamma) := \prod_{i \in [\![1, \mathcal{N}]\!]} L_T(\Gamma_i)$ such that

$$(\boldsymbol{\xi}_i)_j = (\mathcal{S}_j^{\mathrm{RtR}}(\boldsymbol{\xi}_j, \boldsymbol{\mathcal{F}}_j))_i, \quad \forall j \in B^i, \quad \forall i \in [\![1, \mathcal{N}]\!]. \tag{3.9}$$

Using the relation $\mathcal{M}_j(\boldsymbol{\xi}_j, \boldsymbol{\mathcal{F}}_j) = \mathcal{M}_j(\boldsymbol{\xi}_j, \mathbf{0}) + \mathcal{M}_j(\mathbf{0}, \boldsymbol{\mathcal{F}}_j)$ as well as the linearity of the operator $\mathcal{R}_i$ and defining

$$\mathcal{S}_R : \begin{array}{ccc} L_T(\Gamma) & \rightarrow & L_T(\Gamma) \\ \boldsymbol{\xi} & \rightarrow & \left(\left((\boldsymbol{\xi}_i)_j - (\mathcal{S}_j^{\mathrm{RtR}}(\boldsymbol{\xi}_j, \mathbf{0}))_i \right)_{j \in B^i} \right)_{1 \leq i \leq \mathcal{N}}, \end{array} \tag{3.10}$$

and

$$\boldsymbol{\chi} := \left(\left((\mathcal{S}_j^{\mathrm{RtR}}(\mathbf{0}, \boldsymbol{\mathcal{F}}_j))_i \right)_{j \in B^i} \right)_{1 \leq i \leq \mathcal{N}},$$

problem (3.9) can be rewritten as:

$$\mathcal{S}_R \boldsymbol{\xi} = \boldsymbol{\chi}. \tag{3.11}$$

The interface problem (3.11) is usually solved by iterative methods such as block-Jacobi iterations, which correspond to the optimized Schwarz waveform relaxation (OSWR) algorithm, or Krylov-type methods like GMRES (see e.g. [3] for details).

3.2   The fully discrete and nonconforming-in-time interface problem

In this part, after introducing some notations, we present the fully discrete counterpart of the interface problem (3.11), using the lowest-order mixed finite element method (MFE) in space and the discontinuous Galerkin method of order zero in time (DG0) [60]. In the case of different time meshes in different subdomains, the semi-discrete in time counterpart of (3.11) is analyzed in [36, 37] where it is shown that the method preserves the order of the discontinuous Galerkin method. This result is shown numerically in the context of the MFE method in [39]. Recall that for piecewise-constant-in-time source term f, the DG0-in-time scheme corresponds to the backward Euler scheme.

3.2.1   Notations

Some more notations will be needed here.

Time discretization

Let E be a space of functions defined on a subset D of Ω (typically a subdomain or an interface) and let $v(\cdot, t)$ be a function taking its values in E. We denote $P_{\mathcal{T}_{\tau,i}}^0(E)$ the vector space such that $v(\mathbf{x}, \cdot)$, $\mathbf{x} \in D$, is piecewise constant in time:

$$P_{\mathcal{T}_{\tau,i}}^0(E) := \{v(\cdot, t) : (0, T) \rightarrow E; \ v(\cdot, t) \text{ is constant on } I_{n,i}, \ 1 \leq n \leq N_i\}. \tag{3.12}$$

A function in $P_{\mathcal{T}_{\tau,i}}^0(E)$ is thus defined by the N_i functions $\{v^n := v(\cdot, t)|_{I_{n,i}}\}_{1 \leq n \leq N_i}$ in E. In particular, for the physical data we define $\tilde{f}_i \in P_{\mathcal{T}_{\tau,i}}^0(L^2(\Omega_i))$, $\tilde{g}_{\mathrm{D},i} \in P_{\mathcal{T}_{\tau,i}}^0(L^2(\Gamma_i^{\mathrm{D}}))$, and $\tilde{g}_{\mathrm{N},i} \in P_{\mathcal{T}_{\tau,i}}^0(L^2(\Gamma_i^{\mathrm{N}}))$ such that, for $n = 1, .., N$:

$$\tilde{f}_i|_{I_{n,i}} := \tilde{f}^{n,i}, \quad \tilde{g}_{\mathrm{D},i}|_{I_{n,i}} := \tilde{g}_{\mathrm{D}}^{n,i}, \ \text{ and } \ \tilde{g}_{\mathrm{N},i}|_{I_{n,i}} := \tilde{g}_{\mathrm{N}}^{n,i}, \ 1 \leq n \leq N_i, \tag{3.13}$$

where

$$\tilde{f}^{n,i} := \frac{1}{\tau^{n,i}} \int_{I_{n,i}} f(\cdot, t)\mathrm{dt}, \quad \tilde{g}_{\mathrm{D}}^{n,i} := \frac{1}{\tau^{n,i}} \int_{I_{n,i}} g_{\mathrm{D}}(\cdot, t)\mathrm{dt}, \quad \tilde{g}_{\mathrm{N}}^{n,i} := \frac{1}{\tau^{n,i}} \int_{I_{n,i}} g_{\mathrm{N}}(\cdot, t)\mathrm{dt}.$$

In addition, and especially for Definition 4 below for the a posteriori estimates, we denote $P^1_{\mathcal{T}_{\tau,i}}(E)$ the vector space such that $v(\mathbf{x}, \cdot)$ is continuous and piecewise affine in time:

$$P^1_{\mathcal{T}_{\tau,i}}(E) := \{v(\cdot, t) : (0, T) \to E; \ v(\cdot, t) \in C^0(0, T; E),$$
$$v(\cdot, t) \text{ is affine on } I_{n,i}, \ 1 \le n \le N_i\}. \tag{3.14}$$

Note that a function in $P^1_{\mathcal{T}_{\tau,i}}(E)$ is defined by $N+1$ functions $\{v^n := v(\cdot, t^n)\}_{0 \le n \le N_i}$, and that if $v \in P^1_{\mathcal{T}_{\tau,i}}(E)$, then $\partial_t v \in P^0_{\mathcal{T}_{\tau,i}}(E)$ is such that

$$\partial_t v|_{I_{n,i}} = \frac{1}{\tau^{n,i}}(v^n - v^{n-1}), \ 1 \le n \le N_i. \tag{3.15}$$

Time projections

For a given interface $\Gamma_{i,j}$, we introduce the L^2 projection operator $\Pi_{i,j}$ from $P^0_{\mathcal{T}_{\tau,j}}(L^2(\Gamma_{i,j}))$ onto $P^0_{\mathcal{T}_{\tau,i}}(L^2(\Gamma_{i,j}))$, i.e., for $\phi \in P^0_{\mathcal{T}_{\tau,j}}(L^2(\Gamma_{i,j}))$, $(\Pi_{i,j}\phi)|_{I_{n,i}}$ is the average value of ϕ on $I_{n,i}$, for $n = 1, ..., N_i$:

$$(\Pi_{i,j}\phi)|_{I_{n,i}} = \frac{1}{|I_{n,i}|} \sum_{l=1}^{N_j} \int_{I_{l,j} \cap I_{n,i}} \phi. \tag{3.16}$$

Space discretization

Let $M_{h,i} \times \mathbf{W}_{h,i} \subset L^2(\Omega_i) \times \mathbf{H}(\mathrm{div}, \Omega_i)$ be the Raviart–Thomas–Nédélec mixed finite element spaces of order 0 for each subdomain Ω_i:

$$M_{h,i} := \{q_{h,i} \in L^2(\Omega_i); \ q_{h,i}|_K \in \mathbb{P}^0(K), \ \forall K \in \mathcal{T}_{h,i}\},$$

where $\mathbb{P}^0(K)$ is the space of polynomials of degree 0, and

$$\mathbf{W}_{h,i} := \{\mathbf{v}_{h,i} \in \mathbf{H}(\mathrm{div}, \Omega_i); \ \mathbf{v}_{h,i}|_K \in \mathbf{RTN}_0(K), \ \forall K \in \mathcal{T}_{h,i}\},$$

where $\mathbf{RTN}_0(K) := [\mathbb{P}_0(K)]^d + \mathbf{x}\mathbb{P}_0(K)$, $\mathbf{x} \in \mathbb{R}^d$, is the Raviart–Thomas–Nédélec space of degree zero associated with the element $K \in \mathcal{T}_{h,i}$. Let $|e|$ be the measure of an edge (face if $d = 3$) $e \subset \Gamma^{\mathrm{N}}_i$. We then define

$$\mathbf{W}^0_{h,i} := \left\{\mathbf{w}_{h,i} \in \mathbf{W}_{h,i}; \ \mathbf{w}_{h,i} \cdot \mathbf{n}|_e = 0\right\}, \quad e \subset \Gamma^{\mathrm{N}}_i,$$

$$\mathbf{W}^{g_{\mathrm{N}},n}_{h,i} := \left\{\mathbf{w}_{h,i} \in \mathbf{W}_{h,i}; \ \mathbf{w}_{h,i} \cdot \mathbf{n}|_e = \frac{1}{|e|}\int_e \tilde{g}^{n,i}_{\mathrm{N}} d\gamma\right\}, \quad e \subset \Gamma^{\mathrm{N}}_i, n = 1, ..., N_i,$$

$$\mathbf{W}^{g_{\mathrm{N}}}_{h\tau,i} := \{\mathbf{w}_{h\tau,i} \in P^0_{\mathcal{T}_{\tau,i}}(\mathbf{W}_{h,i}); \ \mathbf{w}_{h\tau,i}|_{I_{n,i}} \in \mathbf{W}^{g_{\mathrm{N}},n}_{h,i}\}.$$

In the following, for each subdomain Ω_i, $p_{h\tau,i}$ is a function in $P^0_{\mathcal{T}_{\tau,i}}(M_{h,i})$ such that, on each element $K \in \mathcal{T}_{h,i}$, $p_{h\tau,i}(\cdot, 0) = \frac{1}{|K|}\int_K p_0 d\mathbf{x}$, and $\mathbf{u}_{h\tau,i}$ is a function in $\mathbf{W}^{g_{\mathrm{N}}}_{h\tau,i}$.

Note that for a function $\mathbf{v}_{h,i} \in \mathbf{W}_{h,i}$ and a given boundary Γ, the normal trace of $\mathbf{v}_{h,i}$ on Γ is in $\mathbb{P}_0(\mathcal{E}^\Gamma_h)$. The discrete spaces for the Robin and physical data are respectively, for $i \in [\![1, \mathcal{N}]\!]$,

$$L_{\mathcal{T}_{\tau,i},h}(\Gamma_i) := \prod_{j \in B^i} P^0_{\mathcal{T}_{\tau,i}}(\mathbb{P}_0(\mathcal{E}^{\Gamma_{i,j}}_h)),$$

$$\boldsymbol{\mathcal{V}}_{\mathcal{T}_{\tau,i}} := P^0_{\mathcal{T}_{\tau,i}}(L^2(\Omega_i)) \times P^0_{\mathcal{T}_{\tau,i}}(L^2(\Gamma^{\mathrm{D}}_i)) \times P^0_{\mathcal{T}_{\tau,i}}(L^2(\Gamma^{\mathrm{N}}_i)) \times H^1(\Omega_i).$$

3.2.2 Discrete interface problem

The discrete counterpart of the subproblem solution operator $\mathcal{M}_i$, $i \in [\![1, \mathcal{N}]\!]$, from (3.5)–(3.6) is as follows:

$$\mathcal{M}_{h\tau,i}: \begin{array}{ccc} L_{\mathcal{T}_{\tau,i},h}(\Gamma_i) \times \boldsymbol{\mathcal{V}}_{\mathcal{T}_{\tau,i}} & \to & L_{\mathcal{T}_{\tau,i},h}(\Gamma_i) \times P^0_{\mathcal{T}_{\tau,i}}(M_{h,i}) \times \mathbf{W}^{g_{\mathrm{N}}}_{h\tau,i}, \\ (\boldsymbol{\xi}_{h\tau,i}, \boldsymbol{\mathcal{F}}_{\tau,i}) & \to & (\boldsymbol{\xi}_{h\tau,i}, p_{h\tau,i}, \mathbf{u}_{h\tau,i}), \end{array} \tag{3.18}$$

where $\boldsymbol{\xi}_{h\tau,i} := (\boldsymbol{\xi}_{h\tau,i,j})_{j\in B^i} := \left\{ \left(\xi^n_{h,i,j}\right)_{j\in B^i} \right\}_{1\leq n\leq N_i}$ with $\xi^n_{h,i,j}$ being the piecewise space-time constant discrete Robin condition, $\boldsymbol{\mathcal{F}}_{\tau,i} = (\tilde{f}_i, \tilde{g}_{\mathrm{D},i}, \tilde{g}_{\mathrm{N},i}, p_0|_{\Omega_i})$, and where $(p_{h\tau,i}, \mathbf{u}_{h\tau,i})$, $p_{h\tau,i}|_{I_{n,i}} := p^n_{h,i}$, $\mathbf{u}_{h\tau,i}|_{I_{n,i}} := \mathbf{u}^n_{h,i}$, is the solution of the following fully discrete problem in Ω_i: find $\mathbf{u}^n_{h,i} \in \mathbf{W}^{g_{\mathrm{N}},n}_{h,i}$ and $p^n_{h,i} \in M_{h,i}$ on the interval I_n, for $n = 1,..,N_i$, such that:

$$\mathbf{a}_i(\mathbf{u}^n_{h,i}, \mathbf{v}_{h,i}) - \mathbf{b}_i(\mathbf{v}_{h,i}, p^n_{h,i}) = \boldsymbol{\ell}^n_i(\mathbf{v}_{h,i}), \qquad \forall \mathbf{v}_{h,i} \in \mathbf{W}^0_{h,i}, \tag{3.19a}$$

$$\frac{1}{\tau^{n,i}}(p^n_{h,i} - p^{n-1}_{h,i}, q_{h,i})_{\Omega_i} + \mathbf{b}_i(\mathbf{u}^n_{h,i}, q_{h,i}) = (\tilde{f}^{n,i}, q_{h,i})_{\Omega_i}, \qquad \forall q_{h,i} \in M_{h,i}, \tag{3.19b}$$

$$(p^0_{h,i}, q_{h,i})_{\Omega_i} = (p_0, q_{h,i}), \qquad \forall q_{h,i} \in M_{h,i}, \tag{3.19c}$$

where the bilinear forms $\mathbf{a}_i$ and $\mathbf{b}_i$ and the linear form $\boldsymbol{\ell}^n_i$ are defined by:

$$\mathbf{a}_i : \mathbf{W}_{h,i} \times \mathbf{W}_{h,i} \to \mathbb{R}, \ \mathbf{a}_i(\mathbf{u}_{h,i}, \mathbf{v}_{h,i}) := (\boldsymbol{S}^{-1}\mathbf{u}_{h,i}, \mathbf{v}_{h,i})_{\Omega_i} + \sum_{j\in B^i} \langle \beta_{i,j} \mathbf{u}_{h,i}\cdot\mathbf{n}_i, \mathbf{v}_{h,i}\cdot\mathbf{n}_i \rangle_{\Gamma_{i,j}},$$

$$\mathbf{b}_i : \mathbf{W}_{h,i} \times M_{h,i} \to \mathbb{R}, \ \mathbf{b}_i(\mathbf{v}_{h,i}, q_{h,i}) := (q_{h,i}, \nabla\cdot\mathbf{v}_{h,i})_{\Omega_i},$$

$$\boldsymbol{\ell}^n_i : \qquad \mathbf{W}_{h,i} \to \mathbb{R}, \qquad \boldsymbol{\ell}_i(\mathbf{v}_{h,i}) := -\langle \tilde{g}^{n,i}_{\mathrm{D}}, \mathbf{v}_{h,i}\cdot\mathbf{n}_i \rangle_{\Gamma^{\mathrm{D}}_i} - \sum_{j\in B^i} \langle \xi^n_{h,i,j}, \mathbf{v}_{h,i}\cdot\mathbf{n}_i \rangle_{\Gamma_{i,j}}.$$

The discrete counterpart $\mathcal{R}_{h\tau,i}$ of the operator $\mathcal{R}_i$ defined in (3.7) is $\mathcal{R}_{h\tau,i}$:

$$\begin{array}{ccc} L_{\mathcal{T}_{\tau,i},h}(\Gamma_i) \times P^0_{\mathcal{T}_{\tau,i}}(M_{h,i}) \times \mathbf{W}^{g_{\mathrm{N}}}_{h\tau,i} & \to & L_{\mathcal{T}_{\tau,i},h}(\Gamma_i), \\ (\boldsymbol{\xi}_{h\tau,i}, p_{h\tau,i}, \mathbf{u}_{h\tau,i}) & \to & \left(\beta_{j,i}\mathbf{u}_{h\tau,i}\cdot\mathbf{n}_i + (\xi_{h\tau,i,j} + \beta_{i,j}\mathbf{u}_{h\tau,i}\cdot\mathbf{n}_i) \right)_{j\in B^i}. \end{array} \tag{3.20}$$

The discrete Robin-to-Robin operator is then defined as:

$$\mathcal{S}^{\mathrm{RtR}}_{h\tau,i} := \mathcal{R}_{h\tau,i} \circ \mathcal{M}_{h\tau,i} : \ L_{\mathcal{T}_{\tau,i},h}(\Gamma_i) \times \boldsymbol{\mathcal{V}}_{\mathcal{T}_{\tau,i}} \to L_{\mathcal{T}_{\tau,i},h}(\Gamma_i). \tag{3.21}$$

Finally, the discrete counterpart of the space-time interface problem (3.11) is: find $\boldsymbol{\xi}_{h\tau} := (\boldsymbol{\xi}_{h\tau,1}, \ldots, \boldsymbol{\xi}_{h\tau,\mathcal{N}}) \in L_{\mathcal{T}_{\tau,i},h}(\Gamma) := \prod_{i\in[\![1,\mathcal{N}]\!]} L_{\mathcal{T}_{\tau,i},h}(\Gamma_i)$ such that

$$\mathcal{S}_{R,h\tau}\, \boldsymbol{\xi}_{h\tau} = \boldsymbol{\chi}_{h\tau}, \tag{3.22}$$

where

$$\mathcal{S}_{R,h\tau} : \begin{array}{ccc} L_{\mathcal{T}_{\tau,i},h}(\Gamma) & \to & L_{\mathcal{T}_{\tau,i},h}(\Gamma), \\ \boldsymbol{\xi}_{h\tau} & \to & \left(\left((\boldsymbol{\xi}_{h\tau,i})_j - (\mathcal{S}^{\mathrm{RtR}}_{h\tau,j}(\boldsymbol{\xi}_{h\tau,j},\mathbf{0}))_i \right)_{j\in B^i} \right)_{1\leq i\leq\mathcal{N}}, \end{array} \tag{3.23}$$

and

$$\boldsymbol{\chi}_{h\tau} := \left(\left((\mathcal{S}^{\mathrm{RtR}}_{h\tau,j}(\mathbf{0}, \boldsymbol{\mathcal{F}}_{\tau,j}))_i \right)_{j\in B^i} \right)_{1\leq i\leq\mathcal{N}}.$$

Applying the block-Jacobi or the GMRES iteration as in [3] gives rise to the discrete approximations

$$p^k_{h\tau}|_{\Omega_i\times I_{n,i}} := p^{k,n}_{h,i}, \qquad \mathbf{u}^k_{h\tau}|_{\Omega_i\times I_{n,i}} := \mathbf{u}^{k,n}_{h,i}, \quad \forall i\in[\![1,\mathcal{N}]\!], 1\leq n\leq N_i.$$

Remark 1. *As noticed in [3], for time-matching grids, on each iteration of the domain decomposition method, there is a continuity of the normal traces of $\mathbf{u}^k_{h\tau}$ across the edges (faces) if $d = 3$ between two simplices in each subdomain Ω_i but not across the interfaces in Γ_i. The continuity of the normal traces of $\mathbf{u}^k_{h\tau}$ (and of the pressure in the sense of Remark 2 below) will only be satisfied at convergence of the space-time DD algorithm.*

4 General a posteriori error estimate: fully computable upper bound

The purpose of this section is to bound the error using the space-time energy norm given in [61, 24, 25] between the exact solution and the approximate solution on each iteration k of the space-time DD method.

The indicators which bound the error are completely calculable and constructed from the approximate solution $(p_{h\tau}^k, \mathbf{u}_{h\tau}^k)$. We first construct a postprocessing $\tilde{p}_{h\tau}^k$, from which we then obtain a potential reconstruction $s_{h\tau}^k$ on each iteration of the DD algorithm, following [25]. We also construct a subdomain potential reconstruction $\overline{s}_{h\tau,i}^k$ for each subdomain Ω_i, $\forall i \in [\![1, \mathcal{N}]\!]$, on each iteration of the DD algorithm, following the idea presented in [3], so as to distinguish the error from $H_0^1(\Omega)$-nonconformity and from domain decomposition. Then, using the same idea of extracting bands and solving local Neumann problems as presented in [3] to evaluate the error in the $\mathbf{H}(\mathrm{div}, \Omega)$-nonconformity, we build a flux reconstruction $\boldsymbol{\sigma}_{h\tau}^k$ on each iteration of the DD algorithm. Then, the space discretization error, the time discretization error, and the domain decomposition error are distinguished.

We first introduce the broken Sobolev space $H^1(\mathcal{T}_h) := \{v \in L^2(\Omega); v|_K \in H^1(K), \forall K \in \mathcal{T}_h\}$ and define the energy semi-norm on $H^1(\mathcal{T}_h)$ by

$$|||\varphi|||^2 := \sum_{K \in \mathcal{T}_h} |||\varphi|||_K^2 := \sum_{K \in \mathcal{T}_h} \|\boldsymbol{S}^{\frac{1}{2}} \nabla \varphi\|_K^2,$$

for all $\varphi \in H^1(\mathcal{T}_h)$, and the energy norm on $\mathbf{L}^2(\Omega)$ by

$$|||\mathbf{v}|||_\star^2 := \sum_{K \in \mathcal{T}_h} |||\mathbf{v}|||_{\star,K}^2 := \sum_{K \in \mathcal{T}_h} \|\boldsymbol{S}^{-\frac{1}{2}} \mathbf{v}\|_K^2,$$

for all $\mathbf{v} \in \mathbf{L}^2(\Omega)$. Then, for a given function v, we let its jump and average be defined respectively by

$$\begin{cases} [\![v]\!] := v|_K - v|_{K'} \text{ and } \{\!\{v\}\!\} := \dfrac{1}{2}(v|_K + v|_{K'}) & \text{if } e \in \left(\underset{j \in B^i}{\cup} \mathcal{E}_h^{\Gamma_{i,j}} \right) \cup \mathcal{E}_{h,i}^{\mathrm{int}}, \\[2ex] [\![v]\!] := v|_e - g_\mathrm{D} \text{ and } \{\!\{v\}\!\} := \dfrac{1}{2}(v|_e + g_\mathrm{D}) & \text{if } e \in \mathcal{E}_{h,i}^{\Gamma_\mathrm{D}}. \end{cases}$$

In what follows, for $D \subset \Omega$, we denote respectively by $c_{\boldsymbol{S},D}$, $C_{\boldsymbol{S},D}$ the smallest and the largest eigenvalue of the tensor $\boldsymbol{S}$ in D. Finally, for the forthcoming theorems, we will use the Poincaré inequality: for $K \in \mathcal{T}_h$, since K is convex, we have:

$$\|\varphi - \pi_0 \varphi\|_K \le \frac{h_K}{\pi} \|\nabla \varphi\|_K \qquad \forall \varphi \in H^1(K), \tag{4.1}$$

where $\pi_0 \varphi$ is the mean value of φ on K.

4.1 Construction of the unknown values of $(p_{h\tau,i}^k, \mathbf{u}_{h\tau,i}^k)$ on $\mathcal{T}_{\tau,j}$, $j \in B^i$

At the iteration k of the DD algorithm, when different time grids are employed in different subdomains, we obtain $\forall i \in [\![1, \mathcal{N}]\!]$ the couple $(p_{h,i}^{k,n}, \mathbf{u}_{h,i}^{k,n})$ on each time step $t^{n,i}$, $1 \le n \le N_i$. Here, $t^{n,i} \neq t^{n,j}$ for $j \in B^i$ in general, and, consequently, the couples $(p_{h,i}^{k,n}, \mathbf{u}_{h,i}^{k,n})$ for $1 \le n \le N_i$ are not approximations at the same times as $(p_{h,j}^{k,n}, \mathbf{u}_{h,j}^{k,n})$, $1 \le n \le N_j$. For our a posteriori error analysis, we first need to define these approximations pairs on the common refinement of all individual time grids $\mathcal{T}_\tau$ defined in Section 2.2. To do so, for $i \in [\![1, \mathcal{N}]\!]$, $1 \le n \le N_i$, we first compute the number R of the new time steps between $t^{n-1,i}$ and $t^{n,i}$. Let $t^{m-1} = t^{n-1,i}$ and $t^{m+R} = t^{n,i}$ be the two successive time steps in $\{t^{n,i}\}_{0 \le n \le N_i}$ where the couples $(p_{h,i}^{k,m-1}, \mathbf{u}_{h,i}^{k,m-1})$ and $(p_{h,i}^{k,m+R}, \mathbf{u}_{h,i}^{k,m+R})$ are known. We then compute the couple $(p_{h,i}^{k,m-1+r}, \mathbf{u}_{h,i}^{k,m-1+r})$ for $r = 1, .., R$ by:

$$\begin{aligned} \mathbf{u}_{h,i}^{k,m-1+r} &:= \mathbf{u}_{h,i}^{k,m-1} + \frac{r}{R+1}(\mathbf{u}_{h,i}^{k,m+R} - \mathbf{u}_{h,i}^{k,m-1}), \\ p_{h,i}^{k,m-1+r} &:= p_{h,i}^{k,m-1} + \frac{r}{R+1}(p_{h,i}^{k,m+R} - p_{h,i}^{k,m-1}). \end{aligned} \tag{4.2}$$

Note that this is a simple explicit postprocessing step. Generalizing (3.12) and (3.14), we define the following two spaces for the intersection time grid $\mathcal{T}_\tau$:

$$P_{\mathcal{T}_\tau}^0(E) := \{v(\cdot, t): (0, T) \to E; v(\cdot, t) \text{ is constant on } I_n, \ 1 \le n \le N\},$$
$$P_{\mathcal{T}_\tau}^1(E) := \{v(\cdot, t): (0, T) \to E; v(\cdot, t) \in C^0(0, T; E), v(\cdot, t) \text{ is affine on } I_n, \ 1 \le n \le N\}.$$

4.2   Postprocessing of the approximate solution

We first introduce a postprocessing as described in [8, 5, 62]; in our case, we apply it on each time step. We in particular construct $\tilde{p}_{h,i}^{k,n} \in \mathbb{P}_2(\mathcal{T}_{h,i})$ for each subdomain $i \in [\![1, \mathcal{N}]\!]$, on each iteration k, and on each time step n of the intersection time grid $\mathcal{T}_\tau$, $0 \leq n \leq N$, such that:

$$-\boldsymbol{S}\nabla\tilde{p}_{h,i}^{k,n}|_K = \mathbf{u}_{h,i}^{k,n}|_K, \qquad \forall K \in \mathcal{T}_{h,i}, \tag{4.4a}$$

$$\pi_0(\tilde{p}_{h,i}^{k,n}|_K) = p_{h,i}^{k,n}|_K, \qquad \forall K \in \mathcal{T}_{h,i}. \tag{4.4b}$$

Therefrom, denoting as usual $\tilde{p}_h^{k,n}|_{\Omega_i} = \tilde{p}_{h,i}^{k,n}$, we build the postprocessing of the approximate solution for which we will perform the a posteriori error analysis, a discontinuous piecewise second-order polynomial in space and continuous piecewise affine in time:

$$\tilde{p}_{h\tau}^k \in P_{\mathcal{T}_\tau}^1(\mathbb{P}_2(\mathcal{T}_h)), \quad \tilde{p}_{h\tau}^k(\cdot, t^n) := \tilde{p}_h^{k,n}.$$

Remark 2. *As discussed in [62], $\tilde{p}_h^{k,n}|_{\Omega_i} \notin H^1(\Omega_i)$ but is weakly continuous, i.e., $\langle [\![\tilde{p}_h^{k,n}]\!], 1\rangle_e = 0$ on the interior edges $e \in \mathcal{E}_{h,i}^{\mathrm{int}}$ but not on the edges $e \in \mathcal{E}_h^{\Gamma_{i,j}}$ located on the interface. Only at convergence and for a conforming time grid, we obtain the weak continuity $\langle [\![\tilde{p}_h^{k,n}]\!], 1\rangle_e = 0$ for $e \in \mathcal{E}_h^{\Gamma_{i,j}}$.*

4.3   Concept of potential and flux reconstruction for the heat equation

The main idea of our estimation is to construct the following three auxiliary objects on each iteration k, $k \geq 0$, of the global-in-time DD algorithm: $s_{h\tau}^k$, $\overline{s}_{h\tau}^k$, and $\boldsymbol{\sigma}_{h\tau}^k$. These reconstructions will be the central tools used in Theorem 6 below.

Definition 3 (Subdomain potential reconstruction)**.** *We will call a* subdomain potential reconstruction, *for Ω_i, $i \in [\![1, \mathcal{N}]\!]$, any function $\overline{s}_{h\tau,i}^k$ constructed from $\tilde{p}_{h\tau,i}^k$ such that*

- *it is subdomain $H^1(\Omega_i)$-conforming in space, continuous and piecewise affine in time, i.e.,*

$$\overline{s}_{h\tau,i}^k \in P_{\mathcal{T}_\tau}^1(H^1(\Omega_i) \cap C^0(\overline{\Omega}_i)), \tag{4.5a}$$

$$\overline{s}_{h\tau,i}^k|_{\Gamma_i^{\mathrm{D}}} = g_{\mathrm{D}}|_{\Gamma_i^{\mathrm{D}}}; \tag{4.5b}$$

- *on each time step n of the common refinement temporal mesh $\mathcal{T}_\tau$, $0 \leq n \leq N$, the mean values of $\tilde{p}_{h,i}^{k,n}$ are preserved,*

$$(\overline{s}_{h,i}^{k,n}, 1)_K = (\tilde{p}_{h,i}^{k,n}, 1)_K, \;\; \forall K \in \mathcal{T}_{h,i}, \tag{4.6}$$

where $\overline{s}_{h,i}^{k,n} := \overline{s}_{h\tau,i}^k(\cdot, t^n)$;

- *it is built locally subdomain by subdomain to capture the nonconformity from the numerical scheme by comparing it with $\tilde{p}_{h\tau}^k$ in the sense that the estimators (4.16d), and (4.16g), as well as (4.16b) below, (recall (4.4a) which explains the comparison of the fluxes $-\boldsymbol{S}\nabla\overline{s}_h^{k,n}$ and $\mathbf{u}_h^{k,n}$) are as small as possible.*

Definition 4 (Potential reconstruction)**.** *We will call a* potential reconstruction *any function $s_{h\tau}^k$ constructed from $\tilde{p}_{h\tau}^k$ such that*

- *it is globally $H^1(\Omega)$-conforming in space, continuous and piecewise affine in time, i.e.,*

$$s_{h\tau}^k \in P_{\mathcal{T}_\tau}^1(H^1(\Omega) \cap C^0(\overline{\Omega})), \tag{4.7a}$$

$$s_{h\tau}^k|_{\Gamma^{\mathrm{D}}} = g_{\mathrm{D}}; \tag{4.7b}$$

- *on each time step n of the common refinement temporal mesh $\mathcal{T}_\tau$, $0 \leq n \leq N$, the mean values of $\tilde{p}_h^{k,n}$ are preserved,*

$$(s_h^{k,n}, 1)_K = (\tilde{p}_h^{k,n}, 1)_K, \;\; \forall K \in \mathcal{T}_h, \tag{4.8}$$

where $s_h^{k,n} := s_{h\tau}^k(\cdot, t^n)$;

- *its comparison with $\bar{s}_{h\tau}^k$ of Definition 3 estimates the domain decomposition error in the sense that*
$$\left\{ \int_0^T |||\bar{s}_{h\tau}^k - s_{h\tau}^k|||^2 \mathrm{d}t \right\}^{\frac{1}{2}} \to 0 \quad and \quad \left\{ \int_0^T ||\partial_t(\bar{s}_{h\tau}^k - s_{h\tau}^k)||^2 \mathrm{d}t \right\}^{\frac{1}{2}} \to 0 \quad when \ k \to \infty \ in \ the \ case \ of \ a$$
conforming time grid.

Definition 5 (Equilibrated flux reconstruction). *We will call an* equilibrated flux reconstruction *any function $\boldsymbol{\sigma}_{h\tau}^k$ constructed from $\tilde{p}_{h\tau}^k$, $\mathbf{u}_{h\tau}^k$, such that*

- *it is $\mathbf{H}(\mathrm{div})$-conforming and locally conservative in space, piecewise constant in time, i.e.,*
$$\boldsymbol{\sigma}_{h\tau}^k \in P_{\mathcal{T}_\tau}^0(\mathbf{H}(\mathrm{div}, \Omega)); \tag{4.9}$$

- *it has a local conservation property on each time step n of $\mathcal{T}_\tau$, $0 \le n \le N$:*
$$(\tilde{f}^n - \partial_t \tilde{p}_{h\tau}^k|_{I_n} - \nabla \cdot \boldsymbol{\sigma}_h^{k,n}, 1)_K = 0, \quad \forall K \in \mathcal{T}_h, \tag{4.10}$$

together with the Neumann condition:
$$-(\boldsymbol{\sigma}_h^{k,n} \cdot \mathbf{n}_\Omega, 1)_e = (\tilde{g}_N, 1)_e, \qquad \forall e \in \bigcup_{i=1}^{\mathcal{N}} \mathcal{E}_{h,i}^{\Gamma^N}, \tag{4.11}$$

where, recall, by convention, $\boldsymbol{\sigma}_h^{k,n} := \boldsymbol{\sigma}_{h\tau}^k|_{I_n}$;

- *its comparison with $\mathbf{u}_{h\tau}^k$ can be used to estimate the DD error in the sense that $\left\{ \int_0^T |||\mathbf{u}_{h\tau}^k - \boldsymbol{\sigma}_{h\tau}^k|||_\star^2 \mathrm{d}t \right\}^{\frac{1}{2}} \to 0$ when $k \to \infty$ in the case of a conforming time grid.*

4.4 Fully computable upper bound

Let $X := L^2(0, T; H_0^1(\Omega))$ and $X' = L^2(0, T; H^{-1}(\Omega))$; we consider $\Gamma^N = \emptyset$ and $g_D = 0$ in this section for simplicity, knowing that all the results can be extended to the general case proceeding as in, see, e.g., [22], see also the references therein. To work with the nonconforming approximation $\tilde{p}_{h\tau}^k$ of Section 4.2, we introduce the broken X-norm where ∇ is the broken gradient operator:

$$|||q|||_X^2 := \sum_{n=1}^N \int_{I_n} ||\boldsymbol{S}^{\frac{1}{2}} \nabla q(\cdot, t)||^2 \mathrm{d}t = \sum_{n=1}^N \int_{I_n} \sum_{K \in \mathcal{T}_h} ||\boldsymbol{S}^{\frac{1}{2}} \nabla q(\cdot, t)||_K^2 \, \mathrm{d}t.$$

Let $Y := \{q \in X; \partial_t q \in X'\}$. For $q \in Y$, we will use the space-time norm proposed in [24]:

$$|||q|||_Y^2 := |||q|||_X^2 + ||\partial_t q||_{X'}^2 + ||q(\cdot, T)||^2, \tag{4.12}$$

where

$$||\partial_t q||_{X'} := \left\{ \int_0^T ||\partial_t q||_{H^{-1}(\Omega)}^2 \, \mathrm{d}t \right\}^{\frac{1}{2}} := \left\{ \int_0^T \left(\sup_{v \in H_0^1(\Omega); \, ||\boldsymbol{S}^{\frac{1}{2}} \nabla v|| = 1} \langle \partial_t q, v \rangle \right)^2 \mathrm{d}t \right\}^{\frac{1}{2}},$$

and we again extend the Y-norm and the X' norm to piecewise regular-in-space functions only since $\tilde{p}_{h\tau} \notin X$. By the weak solution of problem (1.1) under the above assumptions, we then understand $p \in Y$ such that $p(\cdot, 0) = p_0$ and

$$\int_0^T \{\langle \partial_t p, v \rangle + (\boldsymbol{S} \nabla p, \nabla v)\} \, \mathrm{d}t = \int_0^T (f, v) \, \mathrm{d}t \qquad \forall v \in X. \tag{4.13}$$

Our main result is then:

Theorem 6 (A posteriori error estimates for the potential, distinguishing space, time, and domain decomposition error components). *Let p be the weak solution of problem (1.1) given by (4.13). Let $\tilde{p}_{h\tau}^k \in P_{\mathcal{T}_\tau}^1(H^1(\mathcal{T}_h))$ be an arbitrary approximation to p; in particular $\tilde{p}_h^{k,n} = \tilde{p}_{h\tau}^k(\cdot, t^n)$ can be the postprocessing (4.4) of the solution $(p_h^{k,n}, \mathbf{u}_h^{k,n})$ at iteration k of the global-in-time Robin DD algorithm (3.19)–(3.22).*

Let $\mathbf{u}_h^{k,n}|_K := -\boldsymbol{S}\nabla\tilde{p}_h^{k,n}|_K$ in each element $K \in \mathcal{T}_h$. Let $\overline{s}_{h\tau,i}^k$ be the subdomain potential reconstruction of Definition 3, let $s_{h\tau}^k$ be the potential reconstruction of Definition 4, and let $\boldsymbol{\sigma}_{h\tau}^k$ be the equilibrated flux reconstruction of Definition 5. Then there holds

$$|||p - \tilde{p}_{h\tau}^k|||_Y \leq \tilde{\eta}^k := \eta_{\mathrm{sp}}^k + \eta_{\mathrm{tm}}^k + \eta_{\mathrm{DD,NC_{tm}}}^k + \eta_{\mathrm{IC}}^k + ||f - \tilde{f}||_{X'}, \tag{4.14}$$

where the "spatial discretization estimator" is

$$\eta_{\mathrm{sp}}^k := \left\{ \sum_{n=1}^N \tau^n \sum_{K \in \mathcal{T}_h} (\eta_{\mathrm{osc},K}^{k,n} + \eta_{\mathrm{DF},1,a,K}^{k,n})^2 \right\}^{\frac{1}{2}} + \left\{ \sum_{n=1}^N \int_{I_n} \sum_{K \in \mathcal{T}_h} (\eta_{\mathrm{NCP},1,a,K}^k(t))^2 \mathrm{d}t \right\}^{\frac{1}{2}}$$

$$+ \left\{ \sum_{n=1}^N \tau^n \sum_{K \in \mathcal{T}_h} (\eta_{\mathrm{NCP},2,a,K}^{k,n})^2 \right\}^{\frac{1}{2}} + ||s_h^{k,N} - \tilde{p}_h^{k,N}||,$$

the "time discretization estimator" is

$$\eta_{\mathrm{tm}}^k := \left\{ \sum_{n=1}^N \sum_{K \in \mathcal{T}_h} \frac{1}{3} \tau^n |||s_h^{k,n} - s_h^{k,n-1}|||_K^2 \right\}^{\frac{1}{2}},$$

the "domain decomposition and nonconformity discretization in time estimator" is

$$\eta_{\mathrm{DD,NC_{tm}}}^k := \left\{ \sum_{n=1}^N \tau^n \sum_{K \in \mathcal{T}_h} (\eta_{\mathrm{DF},1,b,K}^{k,n} + \eta_{\mathrm{NCP},1,b,K}^{k,n})^2 \right\}^{\frac{1}{2}}$$

$$+ \left\{ \sum_{n=1}^N \int_{I_n} \sum_{K \in \mathcal{T}_h} (\eta_{\mathrm{NCP},1,b,K}^k(t))^2 \mathrm{d}t \right\}^{\frac{1}{2}} \tag{4.15}$$

$$+ \left\{ \sum_{n=1}^N \tau^n \sum_{K \in \mathcal{T}_h} (\eta_{\mathrm{NCP},2,b,K}^{k,n})^2 \right\}^{\frac{1}{2}},$$

and the "initial condition estimator" is

$$\eta_{\mathrm{IC}}^k := ||s_h^{k,0} - p_0||.$$

For all $1 \leq n \leq N$ and $K \in \mathcal{T}_h$, the following terms are the elementwise estimators :

$$\eta_{\mathrm{osc},K}^{k,n} := \frac{h_K}{\pi} c_{\boldsymbol{S},K}^{-\frac{1}{2}} ||\tilde{f}^n - \partial_t s_{h\tau}^k|_{I_n} - \nabla\cdot\boldsymbol{\sigma}_h^{k,n}||_K, \quad \text{``data oscillation''}, \tag{4.16a}$$

$$\eta_{\mathrm{DF},1,a,K}^{k,n} := |||\boldsymbol{S}\nabla\overline{s}_h^{k,n} + \mathbf{u}_h^{k,n}|||_{\star,K}, \quad \text{``constitutive relation''}, \tag{4.16b}$$

$$\eta_{\mathrm{DF},1,b,K}^{k,n} := |||\mathbf{u}_h^{k,n} - \boldsymbol{\sigma}_h^{k,n}|||_{\star,K}, \quad \text{``DD flux nonconformity''}, \tag{4.16c}$$

$$\eta_{\mathrm{NCP},1,a,K}^k(t) := |||(\tilde{p}_{h\tau}^k - \overline{s}_{h\tau}^k)(t)|||_K, \ t \in I_n \quad \text{``potential nonconformity''}, \tag{4.16d}$$

$$\eta_{\mathrm{NCP},1,b,K}^k(t) := |||(\overline{s}_{h\tau}^k - s_{h\tau}^k)(t)|||_K, \ t \in I_n \quad \text{``DD potential nonconformity''}, \tag{4.16e}$$

$$\eta_{\mathrm{NCP},1,b,K}^{k,n} := |||\overline{s}_h^{k,n} - s_h^{k,n}|||_K, \ \text{``DD potential nonconformity''}, \tag{4.16f}$$

$$\eta_{\mathrm{NCP},2,a,K}^{k,n} := \frac{h_K}{\pi} c_{\boldsymbol{S},K}^{-\frac{1}{2}} ||\partial_t(\tilde{p}_{h\tau}^k - \overline{s}_{h\tau}^k)|_{I_n}||_K, \ \text{``potential nonconformity''}, \tag{4.16g}$$

$$\eta_{\mathrm{NCP},2,b,K}^{k,n} := \frac{h_K}{\pi} c_{\boldsymbol{S},K}^{-\frac{1}{2}} ||\partial_t(\overline{s}_{h\tau}^k - s_{h\tau}^k)|_{I_n}||_K, \ \text{``DD potential nonconformity''}, \tag{4.16h}$$

where we recall that $c_{\boldsymbol{S},K}$ is the smallest eigenvalue of the tensor $\boldsymbol{S}$ in K.

Proof. Using Theorem 2.1 and (2.7) in [24], for a given $s \in Y$ we have:

$$|||p - s|||_Y^2 = ||\mathcal{R}(s)||_{X'}^2 + ||p_0 - s(\cdot,0)||^2, \tag{4.17}$$

where

$$\|\mathcal{R}(s)\|_{X'} := \sup_{v \in X, \, \||v\||_X = 1} \langle \mathcal{R}(s), v \rangle_{X', X}$$

with the residual of the weak formulation (4.13) given for any $v \in X$ by

$$\langle \mathcal{R}(s), v \rangle_{X', X} := \int_0^T \left\{ (f, v) - \langle \partial_t s, v \rangle - (\boldsymbol{S} \nabla s, \nabla v) \right\} (t) \, \mathrm{d}t.$$

In our case, at iteration k of the DD algorithm, $\tilde{p}_{h\tau}^k \notin Y$. For this reason, we can not apply (4.17) to $\||p - \tilde{p}_{h\tau}^k\||_Y$. Thus, we decompose $\||p - \tilde{p}_{h\tau}^k\||_Y$ into two parts using the triangle inequality and then apply (4.17) to $\||p - s_{h\tau}^k\||_Y$ since $s_{h\tau}^k \in Y$:

$$
\begin{aligned}
\||p - \tilde{p}_{h\tau}^k\||_Y &\leq \||p - s_{h\tau}^k\||_Y + \||s_{h\tau}^k - \tilde{p}_{h\tau}^k\||_Y \\
&\leq \|\mathcal{R}(s_{h\tau}^k)\|_{X'} + \eta_{\mathrm{IC}}^k + \||s_{h\tau}^k - \tilde{p}_{h\tau}^k\||_Y.
\end{aligned}
\tag{4.18}
$$

There remains to give a computable upper bound to $\|\mathcal{R}(s_{h\tau}^k)\|_{X'}$ together with $\||s_{h\tau}^k - \tilde{p}_{h\tau}^k\||_Y$ and then combine these results.

1) Computable upper bound on $\|\mathcal{R}(s_{h\tau}^k)\|_{X'}$

To bound the dual norm $\|\mathcal{R}(s_{h\tau}^k)\|_{X'}$, we proceed as in [25, Lemma 5.2]. Let $v \in X$ with $\||v\||_X = 1$ be fixed. By adding and subtracting $(\boldsymbol{\sigma}_{h\tau}^k, \nabla v)$, using the Green theorem, and adding and subtracting $(\tilde{f}, v)$, we obtain:

$$
\begin{aligned}
\langle \mathcal{R} & (s_{h\tau}^k), v \rangle_{X', X} \\
&= \int_0^T \left\{ (f, v) - (\partial_t s_{h\tau}^k + \nabla \cdot \boldsymbol{\sigma}_{h\tau}^k, v) - (\boldsymbol{S} \nabla s_{h\tau}^k + \boldsymbol{\sigma}_{h\tau}^k, \nabla v) \right\} (t) \, \mathrm{d}t \\
&= \int_0^T \left\{ (f - \tilde{f}, v) + (\tilde{f} - \partial_t s_{h\tau}^k - \nabla \cdot \boldsymbol{\sigma}_{h\tau}^k, v) - (\boldsymbol{S} \nabla s_{h\tau}^k + \boldsymbol{\sigma}_{h\tau}^k, \nabla v) \right\} (t) \, \mathrm{d}t \\
&=: R_1 + R_2 + R_3.
\end{aligned}
$$

First, as $\||v\||_X = 1$, we have $|R_1| \leq \|f - \tilde{f}\|_{X'} \||v\||_X = \|f - \tilde{f}\|_{X'}$. Then, we use the property $s_{h\tau}^k \in P_{\mathcal{T}_\tau}^1(H_0^1(\Omega) \cap C^0(\overline{\Omega}))$ (see (4.7)) for the case where $\Gamma^{\mathrm{N}} = \emptyset$ and $g_{\mathrm{D}} = 0$ together with $\boldsymbol{\sigma}_{h\tau}^k \in P_{\mathcal{T}_\tau}^0(\mathbf{H}(\mathrm{div}, \Omega))$ (see (4.9)) to infer

$$R_2 = \sum_{n=1}^N \int_{I_n} (\tilde{f}^n - \partial_t s_{h\tau}^k|_{I_n} - \nabla \cdot \boldsymbol{\sigma}_h^{k,n}, v(t)) \, \mathrm{d}t.$$

Next, Lemma 3.1 in [25], which is a consequence of (4.7) and (4.8), gives on each time step n, $1 \leq n \leq N$

$$(\partial_t s_{h\tau}^k|_{I_n}, 1)_K = (\partial_t \tilde{p}_{h\tau}^k|_{I_n}, 1)_K, \quad \forall K \in \mathcal{T}_h. \tag{4.19}$$

Then, for all n, $1 \leq n \leq N$, using this property and (4.10), we obtain

$$(\tilde{f}^n - \partial_t s_{h\tau}^k|_{I_n} - \nabla \cdot \boldsymbol{\sigma}_h^{k,n}, 1)_K = 0, \quad \forall K \in \mathcal{T}_h. \tag{4.20}$$

Thus, we can write for a.e. $t \in I_n$ at

$$
\begin{aligned}
(\tilde{f}^n - \partial_t s_{h\tau}^k|_{I_n} - \nabla \cdot \boldsymbol{\sigma}_h^{k,n}, v(t))_K &= (\tilde{f}^n - \partial_t s_{h\tau}^k|_{I_n} - \nabla \cdot \boldsymbol{\sigma}_h^{k,n}, v(t) - \pi_0 v(t))_K \\
&\leq \frac{h_K}{\pi} c_{\boldsymbol{S}, K}^{-\frac{1}{2}} \|\tilde{f}^n - \partial_t s_{h\tau}^k|_{I_n} - \nabla \cdot \boldsymbol{\sigma}_h^{k,n}\|_K \||v\||_K(t),
\end{aligned}
$$

employing the Poincaré inequality (4.1) on each $K \in \mathcal{T}_h$. Finally,

$$R_3 \leq \sum_{n=1}^N \int_{I_n} \sum_{K \in \mathcal{T}_h} \||\boldsymbol{S} \nabla s_{h\tau}^k(t) + \boldsymbol{\sigma}_h^{k,n}\||_{\star, K} \||v\||_K(t).$$

The Cauchy–Schwarz inequality gives by collecting the above estimates

$$|R_2 + R_3| \leq \left\{ \sum_{n=1}^{N} \int_{I_n} \sum_{K \in \mathcal{T}_h} (\eta_{\mathrm{osc},K}^{k,n} + |||\boldsymbol{S}\nabla s_{h\tau}^k(t) + \boldsymbol{\sigma}_h^{k,n}|||_{\star,K})^2 \, \mathrm{d}t \right\}^{\frac{1}{2}}.$$

Using the triangle inequality, we obtain:

$$|||\boldsymbol{S}\nabla s_{h\tau}^k(t) + \boldsymbol{\sigma}_h^{k,n}|||_{\star,K} \leq |||\boldsymbol{S}\nabla(s_{h\tau}^k(t) - s_h^{k,n})|||_{\star,K} + |||\boldsymbol{S}\nabla s_h^{k,n} + \boldsymbol{\sigma}_h^{k,n}|||_{\star,K},$$

which leads to

$$\left\{ \sum_{n=1}^{N} \int_{I_n} \sum_{K \in \mathcal{T}_h} (\eta_{\mathrm{osc},K}^{k,n} + |||\boldsymbol{S}\nabla s_{h\tau}^k(t) + \boldsymbol{\sigma}_h^{k,n}|||_{\star,K})^2 \, \mathrm{d}t \right\}^{\frac{1}{2}}$$

$$\leq \left\{ \sum_{n=1}^{N} \int_{I_n} \sum_{K \in \mathcal{T}_h} (\eta_{\mathrm{osc},K}^{k,n} + |||\boldsymbol{S}\nabla s_h^{k,n} + \boldsymbol{\sigma}_h^{k,n}|||_{\star,K})^2 \, \mathrm{d}t \right\}^{\frac{1}{2}}$$

$$+ \left\{ \sum_{n=1}^{N} \int_{I_n} \sum_{K \in \mathcal{T}_h} |||\boldsymbol{S}\nabla(s_{h\tau}^k(t) - s_h^{k,n})|||_{\star,K}^2 \, \mathrm{d}t \right\}^{\frac{1}{2}},$$

where both terms on the right-hand side can be now integrated in time. Combining the above results and proceeding for the last term as in [61, equation 6.5] ($\int_{I_n}(s - s^n)^2(t)\,\mathrm{d}t = \int_0^1 (s^n - s^{n-1})^2 \tau^n r^2 \mathrm{d}r = (s^n - s^{n-1})^2 \tau^n/3$), we finally obtain the computable upper bound for $||\mathcal{R}(s_{h\tau}^k)||_{X'}$ as follows:

$$||\mathcal{R}(s_{h\tau}^k)||_{X'} \leq \left\{ \sum_{n=1}^{N} \tau^n \sum_{K \in \mathcal{T}_h} (\eta_{\mathrm{osc},K}^{k,n} + |||\boldsymbol{S}\nabla s_h^{k,n} + \boldsymbol{\sigma}_h^{k,n}|||_{\star,K})^2 \right\}^{\frac{1}{2}} + \eta_{\mathrm{tm}}^k + ||f - \tilde{f}||_{X'}. \qquad (4.21)$$

2) Computable upper bound on $|||s_{h\tau}^k - \tilde{p}_{h\tau}^k|||_Y$

We have from the definition (4.12)

$$|||s_{h\tau}^k - \tilde{p}_{h\tau}^k|||_Y^2 = |||s_{h\tau}^k - \tilde{p}_{h\tau}^k|||_X^2 + ||\partial_t(s_{h\tau}^k - \tilde{p}_{h\tau}^k)||_{X'}^2 + ||s_h^{k,N} - \tilde{p}_h^{k,N}||^2. \qquad (4.22)$$

It is clear that

$$|||s_{h\tau}^k - \tilde{p}_{h\tau}^k|||_X^2 = \sum_{n=1}^{N} \int_{I_n} \sum_{K \in \mathcal{T}_h} |||(\tilde{p}_{h\tau}^k - s_{h\tau}^k)(t)|||_K^2 \mathrm{d}t. \qquad (4.23)$$

To bound the middle term in (4.22), we follow Lemma 5.3 in [25]. Let $v \in X$ with $|||v|||_X = 1$ be fixed. As $s_{h\tau}^k$ and $\tilde{p}_{h\tau}^k$ are piecewise affine and continuous in time, we can write:

$$||\partial_t(s_{h\tau}^k - \tilde{p}_{h\tau}^k)||_{X'}^2 = \int_0^T ||\partial_t(s_{h\tau}^k - \tilde{p}_{h\tau}^k)||_{H^{-1}(\Omega)}^2 \, \mathrm{d}t$$

$$= \sum_{n=1}^{N} \int_{I_n} \sup_{v \in H_0^1(\Omega); \, ||\boldsymbol{S}^{\frac{1}{2}}\nabla v|| = 1} (\partial_t(s_{h\tau}^k - \tilde{p}_{h\tau}^k)|_{I_n}, v)^2 \, \mathrm{d}t. \qquad (4.24)$$

Then, since for all $1 \leq n \leq N$ and on each element $K \in \mathcal{T}_h$, the quantity $\partial_t(s_{h\tau}^k - \tilde{p}_{h\tau}^k)|_{I_n}$ has zero mean value by (4.19),

$$||\partial_t(s_{h\tau}^k - \tilde{p}_{h\tau}^k)||_{X'}^2 = \sum_{n=1}^{N} \int_{I_n} \sup_{v \in H_0^1(\Omega); \, ||\boldsymbol{S}^{\frac{1}{2}}\nabla v|| = 1} (\partial_t(s_{h\tau}^k - \tilde{p}_{h\tau}^k)|_{I_n}, v(t) - \pi_0 v(t))^2 \, \mathrm{d}t.$$

Using the Cauchy–Schwarz and Poincaré inequalities, one obtains

$$||\partial_t(s_{h\tau}^k - \tilde{p}_{h\tau}^k)||_{X'}^2 \leq \sum_{n=1}^{N} \int_{I_n} \left\{ \sum_{K \in \mathcal{T}_h} \left(\frac{h_K}{\pi} c_{\boldsymbol{S},K}^{-\frac{1}{2}} ||\partial_t(s_{h\tau}^k - \tilde{p}_{h\tau}^k)|_{I_n}||_K \right)^2 |||v|||^2 \right\} \mathrm{d}t, \qquad (4.25)$$

where the right-hande side can be easily integrated in time. Finally, using $|||v|||_X = 1$ and from (4.22), (4.23), and (4.25), we obtain:

$$
\begin{aligned}
|||s_{h\tau}^k - \tilde{p}_{h\tau}^k|||_Y^2 \leq {} & \sum_{n=1}^N \int_{I_n} \sum_{K \in \mathcal{T}_h} |||(\tilde{p}_{h\tau}^k - s_{h\tau}^k)(t)|||_K^2 \mathrm{d}t \\
& + \sum_{n=1}^N \tau^n \sum_{K \in \mathcal{T}_h} \left(\frac{h_K}{\pi} c_{\boldsymbol{S},K}^{-\frac{1}{2}} ||\partial_t (s_{h\tau}^k - \tilde{p}_{h\tau}^k)|_{I_n}||_K \right)^2 \\
& + ||s_h^{k,N} - \tilde{p}_h^{k,N}||^2.
\end{aligned}
\tag{4.26}
$$

3) Final bound

The final bound follows from (4.18), (4.21), and (4.26) by triangle inequalities, while distinguishing the error components due to discretization in time η_{tm}^k, the discretization in space η_{sp}^k, the global-in-time DD method $\eta_{\mathrm{DD,NC_{tm}}}^k$, the initial condition η_{IC}^k, and data oscillation $||f - \tilde{f}||_{X'}$. $\qquad\square$

Remark 7. *The estimator $\eta_{\mathrm{DD,NC_{tm}}}$ mixes the error due to the global-in-time domain decomposition method with the possible nonconformity discretization in time. Indeed, there is in particular no reason for $\eta_{\mathrm{DF},1,b,K}^{k,n}$ given in (4.16c), which is part of $\eta_{\mathrm{DD,NC_{tm}}}^k$, to converge to zero for $k \to \infty$ for nonconforming-in-time grids. Indeed, $\boldsymbol{\sigma}_h^{k,n}$ satisfies the local conservation (4.10) on each element K in space, but this is not necessarily the case for $\mathbf{u}_h^{k,n}$ on nonconforming-in-time grids. In the case of the same time grid in all the subdomains, however, $\eta_{\mathrm{DD,NC_{tm}}}$ vanishes at the convergence of the DD algorithm.*

5 Potential and flux reconstructions for the global-in-time DD in the MFE method

In this section, we propose concrete candidates for the reconstructions $\bar{s}_{h,i}^{k,n}$, $s_h^{k,n}$, and $\boldsymbol{\sigma}_h^{k,n}$ of Definitions 3–5, so that Theorem 6 becomes practical. Let $1 \leq n \leq N$ be fixed.

5.1 Potential reconstruction

Let $\mathcal{T}_{\mathbf{a}} := \{K \in \mathcal{T}_h; \mathbf{a} \in K\}$ be the set of the elements K that share the given vertex $\mathbf{a}$ from the set of vertices $\mathcal{V}_h$, and $|\mathcal{T}_{\mathbf{a}}|$ its cardinality. In order to build a potential reconstruction $s_h^{k,n}$ which is $H^1(\Omega)$-conforming in space as indicated in (4.7) and which satisfies the mean value constraint (4.8), we proceed as in [25]. We first apply the averaging operator $\mathcal{I}_{\mathrm{av}} : \mathbb{P}_2(\mathcal{T}_h) \to \mathbb{P}_2(\mathcal{T}_h) \cap H^1(\Omega)$ which associates, to a discontinuous piecewise 2-nd order polynomial $\tilde{p}_h^{k,n} \in \mathbb{P}_2(\mathcal{T}_h)$, a continuous piecewise 2-nd order polynomial $\mathcal{I}_{\mathrm{av}}(\tilde{p}_h^{k,n})$. The value of $\mathcal{I}_{\mathrm{av}}(\tilde{p}_h^{k,n})$ is prescribed at each Lagrange node $\mathbf{a}$ of $\mathbb{P}_2(\mathcal{T}_h) \cap H^1(\Omega)$ by the average of the values of $\tilde{p}_h^{k,n}$ at this node:

$$
\mathcal{I}_{\mathrm{av}}(\tilde{p}_h^{k,n})(\mathbf{a}) := \frac{1}{|\mathcal{T}_{\mathbf{a}}|} \sum_{K \in \mathcal{T}_{\mathbf{a}}} \tilde{p}_h^{k,n}|_K(\mathbf{a});
$$

at the Dirichlet boundary nodes $\mathbf{a}_{\mathrm{D}} \in \Gamma^{\mathrm{D}}$, the value of $\mathcal{I}_{\mathrm{av}}(\tilde{p}_h^{k,n})$ is set to $g_{\mathrm{D}}(\mathbf{a}_{\mathrm{D}})$. In order to obtain (4.8) while maintaining (4.7), we choose $s_h^{k,n}$ as

$$
s_h^{k,n} := \mathcal{I}_{\mathrm{av}}(\tilde{p}_h^{k,n}) + \sum_{K \in \mathcal{T}_h} \alpha_K^{k,n} b_K,
$$

where $\alpha_K^{k,n}$ is chosen as

$$
\alpha_K^{k,n} := \frac{1}{(b_K, 1)_K} (\tilde{p}_h^{k,n} - \mathcal{I}_{\mathrm{av}}(\tilde{p}_h^{k,n}), 1)_K,
\tag{5.1}
$$

and where b_K is the bubble function on the element K. This is a time-independent function defined as the product of the barycentric coordinates of K, so that its value on the boundary ∂K of K is zero.

5.2 Subdomain potential reconstruction

On each iteration k of the DD method, on each time step n, and in each subdomain Ω_i, we have to build the subdomain potential reconstruction $\overline{s}_{h,i}^{k,n}$ which satisfies (4.5a) and (4.6). The construction of the subdomain potential reconstruction $\overline{s}_{h,i}^{k,n}$ is only different from the construction of $s_{h,i}^{k,n}$ at the nodes located on the interface $\Gamma_{i,j}$; our $\overline{s}_{h,i}^{k,n}$ is discontinuous across the interfaces at the beginning of the DD algorithm but coincides with $s_{h,i}^{k,n}$ at the convergence of the DD algorithm for a conforming time grid. In order to obtain $\overline{s}_{h,i}^{k,n}$, we first build a potential reconstruction, denoted $\overline{\overline{s}}_{h,i}^{k,n}$, as in [3], then we add the second part which allows us the verify (4.6).

5.2.1 Notations

We denote by $\mathcal{V}_h^{\Gamma_{i,j}} \subset \mathcal{V}_h$, $i < j$, $i,j \in [\![1, \mathcal{N}]\!]$, the set of vertices located on the interface $\Gamma_{i,j}$. We denote the set of vertices $\mathbf{a} \in \partial\Gamma_{i,j}$ by $\mathcal{V}_h^{\partial\Gamma_{i,j}}$, and the set of vertices $\mathbf{a} \in \Gamma_{i,j}\backslash(\partial\Gamma_{i,j})$ by $\mathcal{V}_h^{\Gamma_{i,j}\backslash(\partial\Gamma_{i,j})}$. Let $I_{\mathbf{a}}$ be the set of interfaces $\Gamma_{i,j}$ that share the vertex $\mathbf{a} \in \mathcal{V}_h^{\partial\Gamma_{i,j}}$: $I_{\mathbf{a}} := \{\Gamma_{i,j} : i < j, \ i,j \in [\![1, \mathcal{N}]\!], \mathbf{a} \in \mathcal{V}_h^{\partial\Gamma_{i,j}}\}$. Let $|I_{\mathbf{a}}|$ be the cardinality of this set and let $I_{\mathbf{a}}^r$ be the rth interface in $I_{\mathbf{a}}$ sharing $\mathbf{a}$. Due to the domain decomposition, $\mathcal{T}_{\mathbf{a}} = \overset{\mathcal{N}}{\underset{i=1}{\cup}}\{K \in \mathcal{T}_{h,i}; \mathbf{a} \in K\} = \overset{\mathcal{N}}{\underset{i=1}{\cup}} \mathcal{T}_{\mathbf{a}}^i$ where $\mathcal{T}_{\mathbf{a}}^i$ is the set of all elements in the subdomain Ω_i sharing the node $\mathbf{a}$; we denote by $|\mathcal{T}_{\mathbf{a}}^i|$ their number. We will also need $\tilde{B}^i$, the set of subdomains other than Ω_i that share at least one vertex with Ω_i, and its cardinality $|\tilde{B}^i|$.

5.2.2 Weights

Using the above notations, we aim to construct weights on the interface on each iteration k of the DD algorithm which depend on the quantities $\langle [\![\tilde{p}_h^{k,n}]\!], 1\rangle_e$, $\forall e \in \mathcal{E}_h^{\Gamma_{i,j}}$, using the fact that $\langle [\![\tilde{p}_h^{k,n}]\!], 1\rangle_e \to 0$ when $k \to \infty$ for conforming time grids on all $e \in \mathcal{E}_h^{\Gamma_{i,j}}$. Following [3], we define the weight of the edge (face) $e \in \mathcal{E}_h^{\Gamma_{i,j}}$ by

$$\overline{w}_e^{k,n} := \left(\frac{|\langle [\![\tilde{p}_h^{k,n}]\!], 1\rangle_e|}{\langle |[\![\tilde{p}_h^{k,n}]\!]|, 1\rangle_e}\right)^{\alpha}, \quad \alpha \geq 1,$$

(note the different position of the absolute value) and the weight on the Lagrange node $\mathbf{a} \in \mathcal{V}_h^{\Gamma_{i,j}}$ located on the interface (in two space dimensions for simplicity) by

$$\overline{w}_{\mathbf{a}}^{k,n} := \begin{cases} \dfrac{1}{2}(\overline{w}_e^{k,n} + \overline{w}_{e'}^{k,n}) & \text{if } \mathbf{a} \in \mathcal{V}_h^{\Gamma_{i,j}\backslash(\partial\Gamma_{i,j})} \text{ where } e,e' \in \mathcal{E}_h^{\Gamma_{i,j}}, e \neq e', e \cap e' = \mathbf{a}, \\ \dfrac{1}{|I_{\mathbf{a}}|}\displaystyle\sum_{r=1}^{|I_{\mathbf{a}}|} \overline{w}_{e_r}^{k,n} & \text{if } \mathbf{a} \in \mathcal{V}_h^{\partial\Gamma_{i,j}} \text{ where } \mathbf{a} \in e_r \subset I_{\mathbf{a}}^r. \end{cases}$$

We note that both $\overline{w}_{\mathbf{a}}^{k,n}$ and $\overline{w}_e^{k,n}$ have similar properties: they are typically close to 1 at the beginning of the DD algorithm and approach 0 during the DD iterations for conforming time grids. This is a consequence of $|\langle [\![\tilde{p}_h^{k,n}]\!], 1\rangle_e| \leq \langle |[\![\tilde{p}_h^{k,n}]\!]|, 1\rangle_e$ which gives $0 \leq \overline{w}_e^{k,n}, \overline{w}_{\mathbf{a}}^{k,n} \leq 1$.

Contrary to the standard averaging operator $\mathcal{I}_{\text{av}}$ in $s_{h,i}^{k,n}$, where the weights are distributed uniformly on each element $K \in \mathcal{T}_{\mathbf{a}}$ sharing the node $\mathbf{a}$ (being equal to $\dfrac{1}{|\mathcal{T}_{\mathbf{a}}|}$), we now want to define weights for the subdomain potential reconstruction $\overline{\overline{s}}_{h,i}^{k,n}$ in the sense of Definition 3 where all elements sharing the same node on the interface do not have the same weight during the iterations of the DD algorithm:

Definition 8 (Weights of Lagrange nodes on the interface for each patch $\mathcal{T}_{\mathbf{a}}^i$)**.** *For each interface Lagrange node* $\mathbf{a} \in \mathcal{V}_h \cap \Gamma_i$, $i \in [\![1, \mathcal{N}]\!]$, *define*

$$w_{i,\mathbf{a}}^{k,n} := \frac{1}{|\mathcal{T}_{\mathbf{a}}^i| + (1 - \overline{w}_{\mathbf{a}}^{k,n})\sum_{j \in \tilde{B}^i} |\mathcal{T}_{\mathbf{a}}^j|}. \tag{5.2}$$

The construction (5.2) ensures that at the beginning of the DD iterations, $w_{i,\mathbf{a}}^{k,n} \approx \dfrac{1}{|\mathcal{T}_{\mathbf{a}}^i|}$, whereas on late DD iterations, $w_{i,\mathbf{a}}^{k,n} \approx \dfrac{1}{|\mathcal{T}_{\mathbf{a}}|}$ for conforming time grids.

5.2.3 Construction of $\overline{s}_{h,i}^{k,n}$

We first build $\overline{\overline{s}}_{h,i}^{k,n}$ as follows:

$$\overline{\overline{s}}_{h,i}^{k,n}(\mathbf{a}) = w_{i,\mathbf{a}}^{k,n} \sum_{K \in \mathcal{T}_{\mathbf{a}}^i} \tilde{p}_{h,i}^{k,n}|_K(\mathbf{a}) + w_{i,\mathbf{a}}^{k,n}(1 - \overline{w}_{\mathbf{a}}^{k,n}) \sum_{j \in \tilde{B}^i} \sum_{K \in \mathcal{T}_{\mathbf{a}}^j} \tilde{p}_{h,j}^{k,n}|_K(\mathbf{a}),$$

where the weights $w_{i,\mathbf{a}}^{k,n}$ and $\overline{w}_{\mathbf{a}}^{k,n}$ presented before are constructed on each time step n. Here, $\overline{\overline{s}}_{h,i}^{k,n}$ satisfies (4.5a): $\overline{\overline{s}}_{h,i}^{k,n} \in H^1(\Omega_i)$; we enforce pointwise the boundary condition (4.5b) for smooth enough g_{D}. It remains to verify the condition (4.6) for $\overline{s}_{h\tau,i}^k$. More precisely, we need the mean value of $\overline{s}_{h,i}^{k,n}$ on each triangle, at time t^n, to be equal to the mean value of the postprocessing $\tilde{p}_{h,i}^{k,n}$ of the discrete solution. For this purpose and while maintaining (4.5a), $\overline{s}_{h,i}^{k,n}$ is chosen as follows:

$$\overline{s}_{h,i}^{k,n} := \overline{\overline{s}}_{h,i}^{k,n} + \sum_{K \in \mathcal{T}_h} \overline{\alpha}_K^{k,n} b_K,$$

where $\overline{\alpha}_K^{k,n} = \dfrac{1}{(b_K, 1)_K}(\tilde{p}_h^{k,n} - \overline{\overline{s}}_{h,i}^{k,n}, 1)_K$ is chosen in the same spirit as in (5.1).

5.3 Flux reconstruction

The domain decomposition with Robin transmission conditions does not give the continuity of the flux $\mathbf{u}_h^{k,n}$ across the interface. Consequently, $\mathbf{u}_h^{k,n}$ is not $\mathbf{H}(\mathrm{div}, \Omega)$-conforming on each time step n. Suppose now that for all interface edges (faces) $e \subset \Gamma_{i,j}$, $\mathbf{n}_e$ has the same direction as the interface normal $\mathbf{n}_{\Gamma_{i,j}}$, where $\mathbf{n}_{\Gamma_{i,j}}$ is set arbitrarily, pointing either from Ω_i to Ω_j, or from Ω_j to Ω_i, with $j \in B^i$, $i < j$, $i \in [\![1, \mathcal{N}]\!]$. Then, defining simply

$$\boldsymbol{\sigma}_h^{k,n} \cdot \mathbf{n}_e = \begin{cases} \{\!\{\mathbf{u}_h^{k,n} \cdot \mathbf{n}_e\}\!\}, & \forall e \in \underset{j \in B^i}{\cup} \mathcal{E}_h^{\Gamma_{i,j}}, \\ \mathbf{u}_{h,i}^{k,n} \cdot \mathbf{n}_e, & \forall e \in \mathcal{E}_{h,i}^{\mathrm{int}} \cup \mathcal{E}_{h,i}^{\mathrm{ext}}, \end{cases} \tag{5.3}$$

leads to (4.9), $\boldsymbol{\sigma}_h^{k,n} \in \mathbf{H}(\mathrm{div}, \Omega)$ on each time step n, as well as (4.11), but not to (4.10) in the elements having an edge (if $d = 2$) or a face (if $d = 3$) on the interface $\Gamma_{i,j}$. Following [3], we now present a procedure allowing to construct an equilibrated flux $\boldsymbol{\sigma}_h^{k,n}$ satisfying (4.9), (4.11), as well as (4.10) on each time step n, relying on interface corrections from a coarse global problem that are further distributed by local problems posed in subdomain bands attached to the interface.

5.3.1 Simple coarse balancing problem

We first partition each subdomain Ω_i, $i \in [\![1, \mathcal{N}]\!]$, into two disjoint parts Ω_i^{ext} and Ω_i^{int} such that $\overline{\Omega_i^{\mathrm{ext}}} \cup \overline{\Omega_i^{\mathrm{int}}} = \overline{\Omega_i}$. The so-called band Ω_i^{ext} is made up of simplices that have an edge, a vertex, or a face on any interface $\Gamma_{i,j}$, $j \in B^i$. We also denote Γ_i^b, $b \in B^{i,\mathrm{ext}}$, the intersections of $\partial\Omega_i^{\mathrm{ext}}$ with $\partial\Omega_i \cap \partial\Omega$ of nonzero $(d-1)$-dimensional measure. We let $B^{i,\mathrm{ext}}$ empty when $|\partial\Omega_i \cap \partial\Omega| = 0$.

Before defining the coarse balancing problem, we evaluate the misfit of the mass balance in each band Ω_i^{ext}, $i \in [\![1, \mathcal{N}]\!]$, due to the averaging in (5.3). Taking $q_{h,i} = 1$ in (3.19b) and then using (3.15) and (4.4b), we have $(\nabla \cdot \mathbf{u}_h^{k,n}, 1)_{\Omega_i} = (\tilde{f}^n - \partial_t \tilde{p}_{h\tau}^k|_{I_n}, 1)_{\Omega_i}$. This also reads

$$(\nabla \cdot \mathbf{u}_h^{k,n}, 1)_{\Omega_i} = (\tilde{f}^n - \partial_t \tilde{p}_{h\tau}^k|_{I_n}, 1)_{\Omega_i^{\mathrm{ext}}} + (\tilde{f}^n - \partial_t \tilde{p}_{h\tau}^k|_{I_n}, 1)_{\Omega_i^{\mathrm{int}}}. \tag{5.4}$$

By taking $q_{h,i} = 1$ in Ω_i^{int} only in (3.19b), the second term in the right-hand side of (5.4) is as follows:
$(\tilde{f}^n - \partial_t \tilde{p}_{h\tau}^k|_{I_n}, 1)_{\Omega_i^{\text{int}}} = (\nabla \cdot \mathbf{u}_h^{k,n}, 1)_{\Omega_i^{\text{int}}}$, and thus replacing this term in (5.4) we obtain

$$(\tilde{f}^n - \partial_t \tilde{p}_{h\tau}^k|_{I_n}, 1)_{\Omega_i^{\text{ext}}} = (\nabla \cdot \mathbf{u}_h^{k,n}, 1)_{\Omega_i} - (\nabla \cdot \mathbf{u}_h^{k,n}, 1)_{\Omega_i^{\text{int}}}.$$

Using the Green theorem in the previous equation leads to

$$(\tilde{f}^n - \partial_t \tilde{p}_{h\tau}^k|_{I_n}, 1)_{\Omega_i^{\text{ext}}} = \langle \mathbf{u}_h^{k,n} \cdot \mathbf{n}_{\partial\Omega_i}, 1 \rangle_{\partial\Omega_i \setminus \Gamma_i} + \langle \mathbf{u}_h^{k,n} \cdot \mathbf{n}_{\partial\Omega_i}, 1 \rangle_{\Gamma_i} - \langle \mathbf{u}_h^{k,n} \cdot \mathbf{n}_{\partial\Omega_i^{\text{int}}}, 1 \rangle_{\partial\Omega_i^{\text{int}}}.$$

Then, adding and subtracting $\langle \boldsymbol{\sigma}_h^{k,n} \cdot \mathbf{n}_{\partial\Omega_i}, 1 \rangle_{\Gamma_i}$ in the previous equation, and using the fact that $\mathbf{n}_{\partial\Omega_i^{\text{int}}} = -\mathbf{n}_{\partial\Omega_i^{\text{ext}}}$ over $\partial\Omega_i^{\text{int}} \cap \partial\Omega_i^{\text{ext}}$ for the last term in the right-hand side, we get

$$(\tilde{f}^n - \partial_t \tilde{p}_{h\tau}^k|_{I_n}, 1)_{\Omega_i^{\text{ext}}} = \langle \boldsymbol{\sigma}_h^{k,n} \cdot \mathbf{n}_{\partial\Omega_i}, 1 \rangle_{\Gamma_i} + \langle (\mathbf{u}_h^{k,n} - \boldsymbol{\sigma}_h^{k,n}) \cdot \mathbf{n}_{\partial\Omega_i}, 1 \rangle_{\Gamma_i}$$
$$- \langle \mathbf{u}_h^{k,n} \cdot \mathbf{n}_{\partial\Omega_i^{\text{int}}}, 1 \rangle_{\partial\Omega_i^{\text{int}}} + \langle \mathbf{u}_h^{k,n} \cdot \mathbf{n}_{\partial\Omega_i}, 1 \rangle_{\partial\Omega_i \setminus \Gamma_i},$$

or, equivalently, using (5.3),

$$\sum_{j \in B^i} \mathbf{n}_{\Gamma_{i,j}} \cdot \mathbf{n}_{\partial\Omega_i^{\text{ext}}} \sum_{e \subset \Gamma_{i,j}} \int_e \frac{1}{2} [\![\mathbf{u}_h^{k,n} \cdot \mathbf{n}_e]\!] \mathrm{d}\gamma = (\tilde{f}^n - \partial_t \tilde{p}_{h\tau}^k|_{I_n}, 1)_{\Omega_i^{\text{ext}}} - \langle \{\!\{\mathbf{u}_h^{k,n} \cdot \mathbf{n}_{\partial\Omega_i^{\text{ext}}} \}\!\}, 1 \rangle_{\partial\Omega_i^{\text{ext}}},$$

which corresponds to the misfit of the mass balance in each band Ω_i^{ext}, $i \in [\![1, \mathcal{N}]\!]$. We now try to correct the averaged interface normal fluxes and the original boundary normal fluxes of (5.3) with one value $c_{\Gamma_{i,j}}^k = c_{\Gamma_{j,i}}^k$ per interface $\Gamma_{i,j} = \Gamma_{j,i}$ and one value $c_{\Gamma_i^b}^k$ per the boundary part Γ_i^b of Γ_i, such that:

$$c_{\Gamma_{i,j}}^{k,n} \approx 0 \qquad \text{for } i, j \in [\![1, \mathcal{N}]\!], \ i < j \text{ such that } j \in B^i, \tag{5.5a}$$

$$c_{\Gamma_i^b}^{k,n} \approx 0 \qquad \text{for } i \in [\![1, \mathcal{N}]\!] \text{ and } b \in B^{i,\text{ext}}, \text{ so that } |\partial\Omega_i^{\text{ext}} \cap \partial\Omega| > 0. \tag{5.5b}$$

On the boundary $\partial\Omega_i^{\text{ext}} \cap \partial\Omega_i^{\text{int}}$, we keep the same value of the flux $\mathbf{u}_h^{k,n} \cdot \mathbf{n}_{\partial\Omega_i^{\text{ext}} \cap \partial\Omega_i^{\text{int}}}$. We require the following $\mathcal{N}$ balancing conditions, one for each band Ω_i^{ext}, to be satisfied:

$$\sum_{b \in B^{i,\text{ext}}} c_{\Gamma_i^b}^{k,n} + \sum_{j \in B^i} (\mathbf{n}_{\Gamma_{i,j}} \cdot \mathbf{n}_{\partial\Omega_i^{\text{ext}}}) c_{\Gamma_{i,j}}^{k,n} = (\tilde{f}^n - \partial_t \tilde{p}_{h\tau}^k|_{I_n}, 1)_{\Omega_i^{\text{ext}}} - \langle \{\!\{\mathbf{u}_h^{k,n} \cdot \mathbf{n}_{\partial\Omega_i^{\text{ext}}} \}\!\}, 1 \rangle_{\partial\Omega_i^{\text{ext}}}.$$

On each time step n, the above equations for $i \in [\![1, \mathcal{N}]\!]$ lead to a rectangular linear system which gives an infinity of solutions. We use the least squares algorithm to obtain the closest solution to (5.5):

$$\sum_{i=1}^{\mathcal{N}} \sum_{b \in B^{i,\text{ext}}} (c_{\Gamma_i^b}^{k,n})^2 + \sum_{i=1}^{\mathcal{N}} \sum_{j \in B^i, \ i < j} (c_{\Gamma_{i,j}}^{k,n})^2 = \min.$$

In place of (5.3), the resulting boundary fluxes are finally

$$\boldsymbol{\sigma}_h^{k,n} \cdot \mathbf{n}_e = \begin{cases} \{\!\{\mathbf{u}_h^{k,n} \cdot \mathbf{n}_e\}\!\} + \dfrac{1}{|\Gamma_{i,j}|} c_{\Gamma_{i,j}}^{k,n}, & \forall e \subset \Gamma_{i,j}, \text{ for } i, j \in [\![1, \mathcal{N}]\!], \ i < j \\ & \qquad \text{such that } j \in B^i, \\ \mathbf{u}_{h,i}^{k,n} \cdot \mathbf{n}_e + \dfrac{1}{|\Gamma_i^b|} c_{\Gamma_i^b}^{k,n}, & \forall e \subset \Gamma_i^b \text{ for } i \in [\![1, \mathcal{N}]\!] \text{ and } b \in B^{i,\text{ext}} \\ & \qquad \text{so that } |\partial\Omega_i^{\text{ext}} \cap \partial\Omega| > 0, \\ \mathbf{u}_{h,i}^{k,n} \cdot \mathbf{n}_e, & \forall e \subset \partial\Omega_i^{\text{ext}} \cap \partial\Omega_i^{\text{int}}, \ i = 1, .., \mathcal{N}, \\ \mathbf{u}_{h,i}^{k,n} \cdot \mathbf{n}_e, & \text{on } \partial\Omega_i \cap \partial\Omega \setminus \Gamma_i^b, \ i = 1, .., \mathcal{N}. \end{cases} \tag{5.6}$$

With these boundary fluxes, the mass balance on each domain Ω_i^{ext} is satisfied on each time step n of the intersection time grid $\mathcal{T}_\tau$.

5.3.2 Solving local Neumann problems in bands

Following [54, Section 3.5.2], we finally solve a well-posed local Neumann problem in each band Ω_i^{ext} and on each time step n, in order to obtain the local conservation property (4.10). This is graphically illustrated in Figure 2, where the bands for the case of two subdomains are highlighted.

Definition 9 (Spaces of the local Neumann problems). *We define in each band Ω_i^{ext}, $i \in [\![1, \mathcal{N}]\!]$, and on each time step $1 \leq n \leq N$ of the intersection time grid $\mathcal{T}_\tau$ the spaces*

$$
\mathbf{W}_{h,z,n,\Omega_i^{\mathrm{ext}}} := \left\{ \mathbf{v}_h \in \mathbf{W}_{h,i}(\Omega_i^{\mathrm{ext}}) : \ \mathbf{v}_h \cdot \mathbf{n}_{\Omega_i^{\mathrm{ext}}} = z + \mathbf{n}_{\partial\Omega_i^{\mathrm{ext}}} \cdot \mathbf{n}_{\Gamma_{i,j}} \frac{c_{\Gamma_{i,j}}^{k,n}}{|\Gamma_{i,j}|} \ if\ z \neq \star,\ 0\ else\ on\ \Gamma_{i,j},\ j \in B^i, \right.
$$

$$
\mathbf{v}_h \cdot \mathbf{n}_{\Omega_i^{\mathrm{ext}}} = z + \frac{c_{\Gamma_i^b}^{k,n}}{|\Gamma_i^b|} \ if\ z \neq \star,\ 0\ else\ on\ \Gamma_i^b,\ b \in B^{i,\mathrm{ext}},
$$

$$
\mathbf{v}_h \cdot \mathbf{n}_{\Omega_i^{\mathrm{ext}}} = z\ if\ z \neq \star,\ 0\ else\ \ on\ \partial\Omega_i^{\mathrm{ext}} \cap \partial\Omega_i^{\mathrm{int}},
$$

$$
\left. \mathbf{v}_h \cdot \mathbf{n}_{\Omega_i^{\mathrm{ext}}} = z\ if\ z \neq \star,\ 0\ else\ \ on\ \partial\Omega_i \cap \partial\Omega \setminus \Gamma_i^b \right\}.
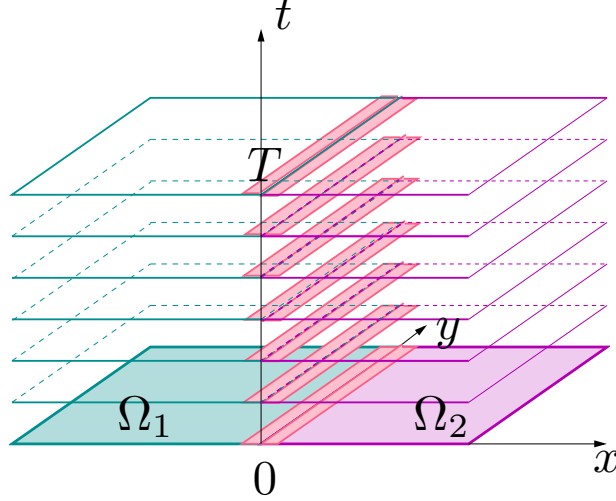$$

Figure 2: Bands in Ω_1 and Ω_2 on each time step

Definition 10 (Mixed finite element local Neumann problems in the bands Ω_i^{ext}). *Find $\boldsymbol{\sigma}_{h\ |\Omega_i^{\mathrm{ext}}}^{k,n} \in \mathbf{W}_{h,\{\!\!\{\mathbf{u}_h^{k,n} \cdot \mathbf{n}_{\Omega_i^{\mathrm{ext}}}\}\!\!\},n,\Omega_i^{\mathrm{ext}}}$ and $q_h^{k,n} \in M_{h,i}(\Omega_i^{\mathrm{ext}})$ such that $(q_h^{k,n}, 1)_{|\Omega_i^{\mathrm{ext}}} = 0$, which solve the following mixed problem:*

$$
(\boldsymbol{S}^{-1}(\boldsymbol{\sigma}_h^{k,n} - \mathbf{u}_h^{k,n}), \mathbf{v}_h)_{\Omega_i^{\mathrm{ext}}} - (q_h^{k,n}, \nabla \cdot \mathbf{v}_h)_{\Omega_i^{\mathrm{ext}}} = 0, \ \ \forall \mathbf{v}_h \in \mathbf{W}_{h,\star,n,\Omega_i^{\mathrm{ext}}},
$$

$$
(\nabla \cdot \boldsymbol{\sigma}_h^{k,n}, w_h)_{\Omega_i^{\mathrm{ext}}} = (\tilde{f}^{n,i} - \partial_t \tilde{p}_{h\tau}^k|_{I_n}, w_h)_{\Omega_i^{\mathrm{ext}}}, \ \ \forall w_h \in M_{h,i}(\Omega_i^{\mathrm{ext}})\ with\ (w_h, 1)_{|\Omega_i^{\mathrm{ext}}} = 0.
$$

5.3.3 Construction of σ_h^k

We finally set, for all $i \in [\![1, \mathcal{N}]\!]$, and for each time step n, $1 \leq n \leq N$, of the intersection time grid $\mathcal{T}_\tau$

$$
\boldsymbol{\sigma}_h^{k,n} := \begin{cases} \boldsymbol{\sigma}_h^{k,n} & \text{on } \Omega_i^{\mathrm{ext}} \text{ via Definition 10,} \\ \mathbf{u}_h^{k,n} & \text{on } \Omega_i^{\mathrm{int}}. \end{cases}
$$

Prescribing $\boldsymbol{\sigma}_{h\tau}^k$ by the N functions $(\boldsymbol{\sigma}_h^{k,n})_{1 \leq n \leq N}$ on the time subintervals $\{I_n\}_{1 \leq n \leq N}$ satisfies all conditions of Definition 5.

6   Numerical results: example in an industrial context

We are concerned with a model problem given by ANDRA, the French National Agency for Radioactive Waste Management (see also [39]), which is a simplified version of a problem that simulates the transport of contaminant in and around a nuclear waste repository site. The simulation domain is depicted in Figure 3 (left) (not to scale). The repository (yellow) where the nuclear waste is stored is a 2950m by 10m rectangle located in the center of a clay domain of 3950m by 140m (light brown). In this example, we consider a more general time-dependent diffusion problem with a discontinuous porosity, $\phi \neq 1$, so the equation is as follows:

$$\mathbf{u} = -\boldsymbol{S}\nabla p \quad \text{in} \quad \Omega \times (0, T), \tag{6.1a}$$

$$\phi \frac{\partial p}{\partial t} + \nabla\cdot\mathbf{u} = f \qquad \text{in} \quad \Omega \times (0, T), \tag{6.1b}$$

where $\Omega = [0, 3950] \times [0, 140]$, p represents the concentration of the contaminant, f is the source term, ϕ is the porosity, and $\boldsymbol{S}$ is the time-independent diffusion tensor. The initial condition is $p_0 = 0$ and we set homogeneous Dirichlet conditions on the top and the bottom of Ω, and homogeneous Neumann conditions on the other sides of $\partial\Omega$. We decompose Ω into nine subdomains where Ω_5 is the nuclear waste repository domain, see Figure 3 (right). For this simulation, we are interested in the long-term behavior of the repository, over one million years, so that we set $T = 10^6$ years. The porosity in Ω is as follows:

$$\phi = \begin{cases} 0.2 & \text{in } \Omega_5, \\ 0.05 & \text{in } \Omega_i, \ i \neq 5, \end{cases} \tag{6.2}$$

the diffusion tensor is:

$$\boldsymbol{S} = \begin{cases} 2 \times 10^{-9}\boldsymbol{I} \text{ m}^2/\text{s} & \text{in } \Omega_5, \\ 5 \times 10^{-12}\boldsymbol{I} \text{ m}^2/\text{s} & \text{in } \Omega_i, \ i \neq 5, \end{cases} \tag{6.3}$$

where $\boldsymbol{I}$ is the identity matrix, and the source term f is zero in the clay layer and

$$f = \begin{cases} 10^{-5}\text{years}^{-1} & \text{if } t \leq 10^5 \text{ years}, \\ 0 & \text{if } t > 10^5 \text{ years}, \end{cases} \quad \text{in the repository.} \tag{6.4}$$

In order to solve our problem easily, we first write below the dimensionless form of (6.1).

6.1   Dimensionless problem

Let (6.1) be the equation defined in $\Omega \times [0, T]$, where $\Omega = [0, X] \times [0, Y]$ and where $\boldsymbol{S}$ is a diagonal matrix: $\begin{bmatrix} \boldsymbol{S}_x & 0 \\ 0 & \boldsymbol{S}_y \end{bmatrix}$. Equations (6.1) can be written now as follows:

$$\mathbf{u} = -\left[\boldsymbol{S}_x \frac{\partial p}{\partial x} \,,\, \boldsymbol{S}_y \frac{\partial p}{\partial y}\right] \quad \text{in} \quad \Omega \times (0, T), \tag{6.5a}$$

$$\phi \frac{\partial p}{\partial t} + \nabla\cdot\mathbf{u} = f \qquad \text{in} \quad \Omega \times (0, T), \tag{6.5b}$$

where $\nabla\cdot\mathbf{u} = -\boldsymbol{S}_x \dfrac{\partial^2 p}{\partial x^2} - \boldsymbol{S}_y \dfrac{\partial^2 p}{\partial y^2}$. We choose characteristic lengths L in x and H in y, a characteristic time t_c, and a characteristic pressure P. The dimensionless variables are: $\tilde{x} = \dfrac{x}{L}$, $\tilde{y} = \dfrac{y}{H}$, $\tilde{t} = \dfrac{t}{t_c}$, so that

$$\frac{\partial}{\partial x} = \frac{\partial}{\partial \tilde{x}}\frac{\partial \tilde{x}}{\partial x} = \frac{1}{L}\frac{\partial}{\partial \tilde{x}} \quad \text{and} \quad \frac{\partial^2}{\partial x^2} = \frac{1}{L^2}\frac{\partial^2}{\partial \tilde{x}^2}, \tag{6.6a}$$

$$\frac{\partial}{\partial y} = \frac{\partial}{\partial \tilde{y}}\frac{\partial \tilde{y}}{\partial y} = \frac{1}{H}\frac{\partial}{\partial \tilde{y}} \quad \text{and} \quad \frac{\partial^2}{\partial y^2} = \frac{1}{H^2}\frac{\partial^2}{\partial \tilde{y}^2}, \tag{6.6b}$$

$$\frac{\partial}{\partial t} = \frac{\partial}{\partial \tilde{t}}\frac{\partial \tilde{t}}{\partial t} = \frac{1}{t_c}\frac{\partial}{\partial \tilde{t}}. \tag{6.6c}$$

Thus, (6.1) becomes:

$$\mathbf{u} = -\left[\frac{\boldsymbol{S}_x}{L} \frac{\partial p}{\partial \tilde{x}} \, , \, \frac{\boldsymbol{S}_y}{H} \frac{\partial p}{\partial \tilde{y}} \right] \quad \text{in} \quad \Omega \times (0, \frac{T}{t_{\mathrm{c}}}), \tag{6.7a}$$

$$\phi \frac{\partial p}{\partial \tilde{t}} + t_{\mathrm{c}} \nabla \cdot \mathbf{u} = t_{\mathrm{c}} f \quad \text{in} \quad \Omega \times (0, \frac{T}{t_{\mathrm{c}}}), \tag{6.7b}$$

where $\nabla \cdot \mathbf{u} = -\tilde{\boldsymbol{S}}_x \frac{\partial^2 p}{\partial \tilde{x}^2} - \tilde{\boldsymbol{S}}_y \frac{\partial^2 p}{\partial \tilde{y}^2}$, with $\tilde{\boldsymbol{S}}_x = \frac{\boldsymbol{S}_x}{L^2}$ and $\tilde{\boldsymbol{S}}_y = \frac{\boldsymbol{S}_y}{H^2}$.

To cope with the anisotropy of the domain, as well as to better visualize the solution and the error distribution in the estimators, we decided to choose $L = 14$, $H = 1$, whereas $t_{\mathrm{c}} = 1$ years $\approx 3.16 \times 10^7 s$. Figure 4 shows an example of the discretization in space for $\tilde{\Omega} := \left[0, \frac{3950}{14} \right] \times [0, 140]$, where the refinement in and around the subdomain $\tilde{\Omega}_5$ containing the nuclear waste is high compared to the other subdomains. In our example, the number of triangles in the mesh $\mathcal{T}_h$ of $\tilde{\Omega}$ is 34984.

Remark 11 (Adaptive DD and mesh refinement). *In this article the mesh is generated with the* `Freefem++` *scientific calculation code [38], without mesh adaptivity, which creates the (not necessary) refinements around the interfaces. An example where the proposed adaptive stopping criterion is combined with adaptive mesh refinement is shown in reference [3], Section 6.3. It illustrates how the reduction in number of DD iterations behaves as the grid is adaptively refined and the discretization error is reduced, using an adaptive initial guess for the DD solver.*
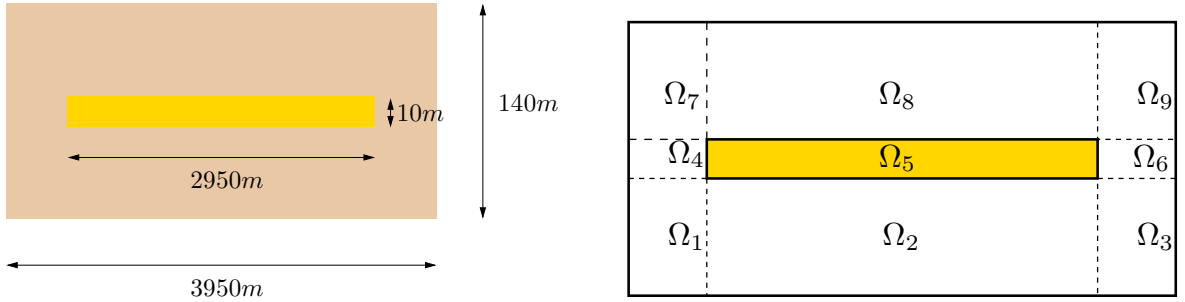

Figure 3: Geometry of the nuclear waste repository (yellow) and the clay layer around it (light brown) on the left and its decomposition into 9 subdomains on the right
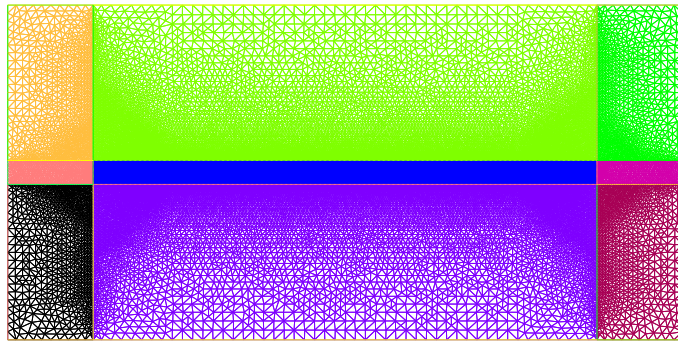

Figure 4: Example of a discretization used in and around a nuclear waste repository site

6.2 An example with global time stepping

In this example, conforming time grids are used such that $\tau^{n,i} = 4000$ years, for all $1 \leq n \leq N_i = 250$, for all subdomain Ω_i, $1 \leq i \leq 9$. Table 1 summarizes the discretization data as well as the stopping criterion.

Number of triangles in $\mathcal{T}_h$	34984
Number of subdomains	9
Subdomain solver	Direct
DD solver	GMRES
Final time	$T = 10^6$ years
Time step $\tau^{n,i}$, $1 \leq i \leq 9$	$10^6/250 = 4000$ years
Original DD stopping criterion	10^{-6}
A posteriori stopping criterion	$\eta^k_{\mathrm{DD,NC_{tm}}} \leq 0.5 \min(\eta^k_{\mathrm{tm}}, \eta^k_{\mathrm{sp}})$
Total number of iterations	28
Number of iterations with a posteriori stopping criterion	8
Unnecessary iterations	20
Spared iteration from the total number of iteration	$\approx 71.42\ \%$

Table 1: Industrial example with conforming time grids and using the GMRES solver
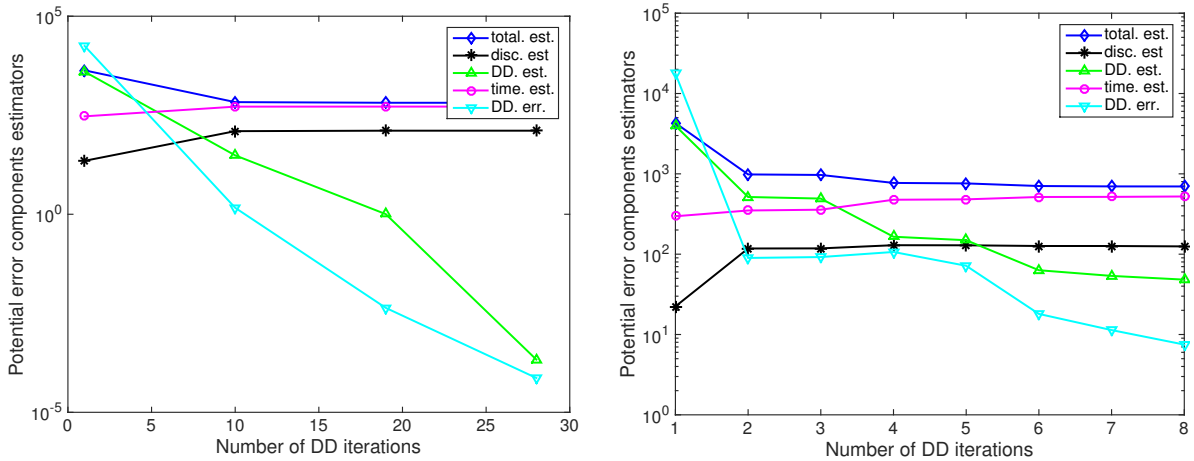

Figure 5: Error component estimates using conforming time grids and with the GMRES solver (left) and zoom until iteration 8 where the a posteriori stopping criterion is satisfied (right)

Figure 5 shows the evolution of our estimators $\eta^k_{\mathrm{DD,NC_{tm}}}$ in green, η^k_{sp} in black, η^k_{tm} in magenta, and their sum in blue as a function of the number of iterations of the DD GMRES solver. In the left figure, these estimators are computed every 9 iterations to decrease the calculation cost. The right figure corresponds to a zoom on the first DD iterations, where the estimators are computed every iteration. We observe that $\eta^k_{\mathrm{DD,NC_{tm}}}$ dominates until iteration 5, then gets smaller compared to η^k_{sp} and η^k_{tm}, and then vanishes, as expected (see Remark 7). Concerning η^k_{sp} and η^k_{tm}, they are approximately constant after iteration 7 and until iteration 28. We have chosen the a posteriori stopping criterion

$$\eta^k_{\mathrm{DD,NC_{tm}}} \leq 0.5 \min(\eta^k_{\mathrm{tm}}, \eta^k_{\mathrm{sp}}), \tag{6.8}$$

leading to 8 iterations, in contrast to the usual stopping criterion, when the jump of the Robin condition on the interface is less than 10^{-6}, satisfied at iteration 28 only.

Figure 5 also shows the evolution of the DD error $|||\tilde{p}^k_{h\tau} - \tilde{p}^\infty_{h\tau}|||_Y$ (approximated by $\{|||\tilde{p}^k_{h\tau} - \tilde{p}^\infty_{h\tau}|||^2_X + ||(\tilde{p}^k_{h\tau} - \tilde{p}^\infty_{h\tau})(\cdot, T)||^2\}^{\frac{1}{2}}$, see Remark 13 below) in cyan, where $\tilde{p}^\infty_{h\tau}$ is the postprocessing of the converged DD solution (computed with a tolerance 10^{-13} on the jump of the Robin condition on the interfaces). Numerically, we can thus observe that our estimate $\eta^k_{\mathrm{DD,NC_{tm}}}$ is an upper bound on the space-time DD error, though we have no theoretical proof for this.

Remark 12 (Stopping criterion)**.** *The rationale of the criterion* (6.8) *is to stop the iterations when the DD error falls below the discretization error, up to a factor here chosen as* 0.5*. This can be ensured when a guaranteed upper bound on the DD error and a guaranteed lower bound on the discretization error are available. Though we do not develop such refined estimates here, they could be obtained following the methodology recently proposed in [52, Section 6.3] and [51, Section 5.2].*

6.3 An example with local time stepping

Here, nonconforming time grids are used such that $\tau^{n,5} = 1000$ years in Ω_5 for all $1 \leq n \leq N_5 = 1000$ and $\tau^{n,i} = 5000$ years for all $1 \leq n \leq N_i = 200$, for $i \neq 5$. The ratio of the number of time discretization steps between the subdomains $\dfrac{N_5}{N_i}$ is 5, for $i \neq 5$. Table 2 summarizes the discretization data as well as the stopping criterion.

Number of triangles in $\mathcal{T}_h$	34984
Number of subdomains	9
Subdomain solver	Direct
DD solver	GMRES
Final time	$T = 10^6$ years
Time step $\tau^{n,i}$, $i \neq 5$	$10^6/200 = 5000$ years
Time step $\tau^{n,i}$, $i = 5$	$10^6/1000 = 1000$ years
Original DD stopping criterion	10^{-6}
A posteriori stopping criterion	$\eta_{\mathrm{DD,NC_{tm}}}^k \leq 0.5 \min(\eta_{\mathrm{tm}}^k, \eta_{\mathrm{sp}}^k)$
Total number of iterations	28
Number of iterations with a posteriori stopping criterion	10
Unnecessary iterations	18
Spared iteration from the total number of iteration	$\approx 64.2\ \%$

Table 2: Industrial example with nonconforming time grids and using the GMRES solver
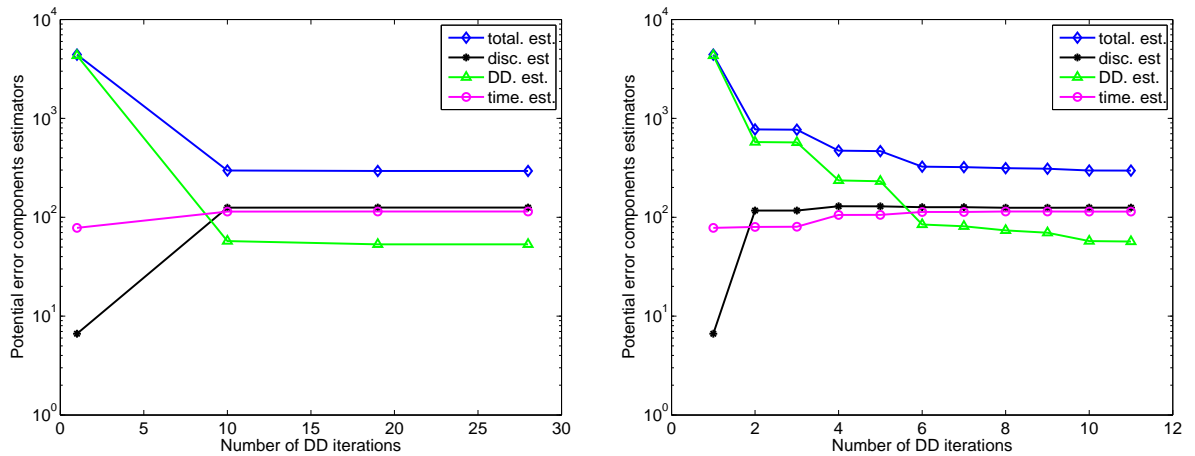

Figure 6: Error component estimates using different time grids and with the GMRES solver (left) and zoom until iteration 10 where the a posteriori stopping criterion is satisfied (right)

The evolution of $\eta_{\mathrm{DD,NC_{tm}}}^k$ in green, η_{sp}^k in black, η_{tm}^k in magenta, and their sum in blue as a function of

the number of iterations of the DD GMRES solver is presented in Figure 6, left. Here again, the estimators are computed every 9 iterations to decrease the calculation cost. We remark in the zoom in the right part of Figure 6 that $\eta^k_{\mathrm{DD,NC_{tm}}}$ dominates until iteration 5 and then decreases again until iteration 10, wherefrom it stagnates. Concerning η^k_{sp} and η^k_{tm}, they are approximately constant after iteration 7 and until iteration 28. We have chosen the a posteriori stopping criterion (6.8) leading to 11 iterations, in contrast to the usual stopping criterion, when the jump of the Robin condition on the interface is less than 10^{-6}, satisfied at iteration 28 only.
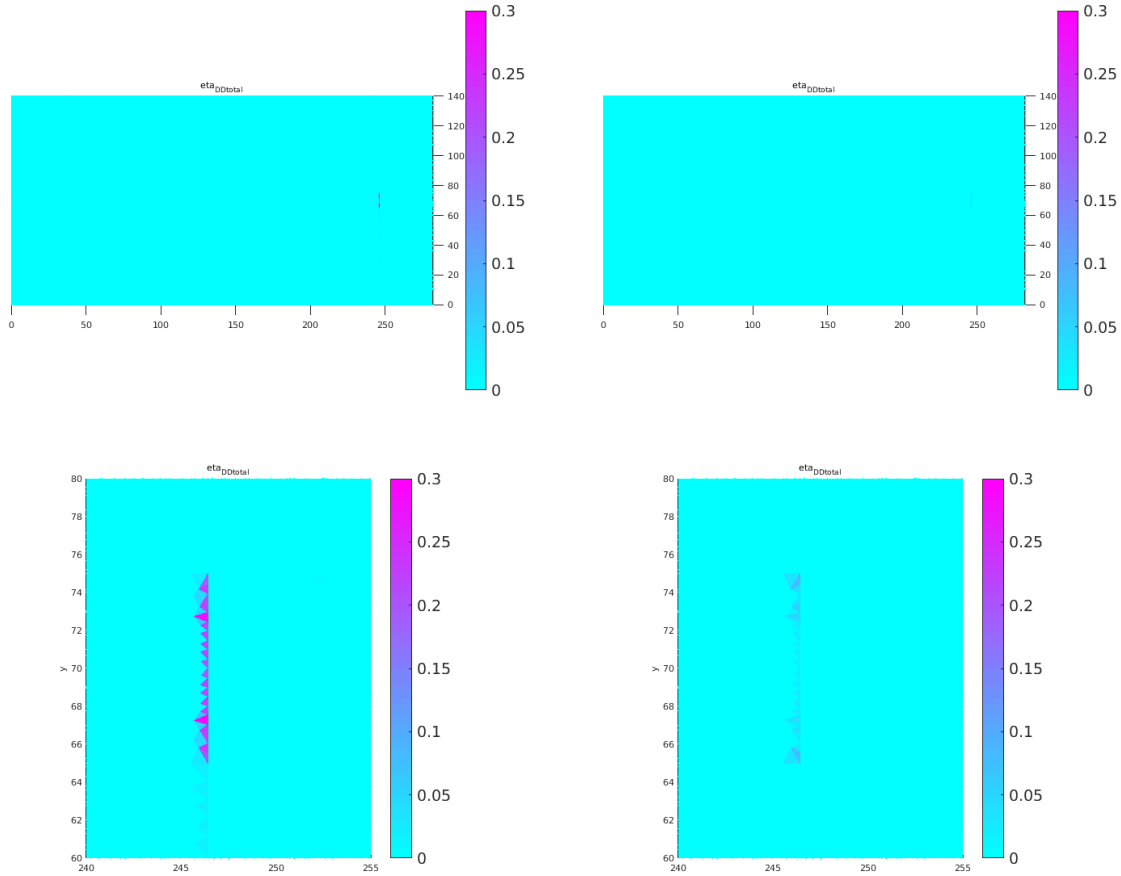

Figure 7: Distribution of $\eta^k_{\mathrm{DD,NC_{tm}}}$ on $\tilde{\Omega}$ at the final time $T = 10^6$ years at iteration 11 (top left), with a zoom on the interface (bottom left) and at iteration 28 (top right) , with a zoom on the interface (bottom right), of the space-time DD algorithm

Figure 7 then presents the elementwise contributions of the estimator $\eta^k_{\mathrm{DD,NC_{tm}}}$ at the final time $T = 10^6$ years at iteration 11 (top left), with a zoom on the interface (bottom left), and at iteration 28 (top right) , with a zoom on the interface (bottom right), of the DD algorithm, respectively. We remark that they decrease slightly but still exist around the interfaces $\Gamma_{5,j}$ at iteration 28. As explained before, see Remark 7, $\eta^k_{\mathrm{DD,NC_{tm}}}$ estimates simultaneously the error due to the domain decomposition and nonconforming time grids; in the first iterations, the DD part dominates, whereas later, the nonconforming time grids part remains. Recall again that $\eta^k_{\mathrm{DD,NC_{tm}}}$ vanishes for global time stepping, see Remark 7 and Section 6.2.

Table 3 gives an insight to the computational cost in the studied test case in Section 6.3. Here, mesh 1 contained 12754 triangular elements, 600 time steps in the subdomain Ω_5, and 120 time steps in the other subdomains, whereas mesh 2 was roughly twice finer with 51054 triangles, 1200 time steps in Ω_5, and 240 time steps elsewhere. Our prototype Matlab implementation uses vectorization following [19] but no parallelism; indeed, most of the evaluation of the estimators can be completely parallelized which can further

drastically decrease the cost. It can be seen from Table 3 that the price of evaluation of our estimators is of the same order as that of DD both in the preparatory phase, carried out before the iterations start, as well as per one DD iteration. It can also be noticed the (decisive) price per iteration decreases for the finer mesh (and shall become negligible in the limit) since in contrast to the DD procedure, it is linear in terms of the number of mesh elements times the number of time steps.

		DD	Estimate	Estimate / DD
Mesh 1	Preparation	0.2	0.7	2.9
	Per iteration	1.4	3.3	2.4
Mesh 2	Preparation	0.8	3.8	4.4
	Per iteration	15.5	24.0	1.5

Table 3: Illustration of time requirements (in seconds): industrial example with nonconforming time grids and using the GMRES solver

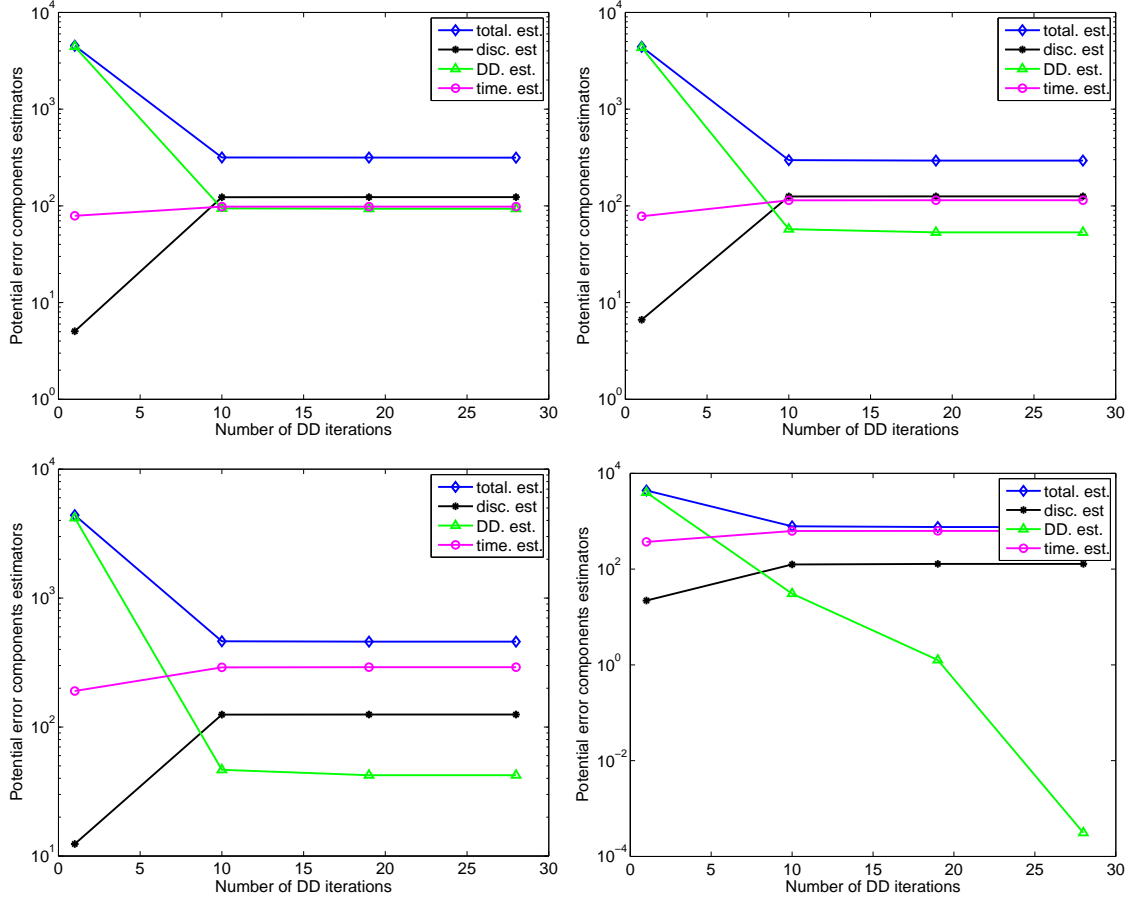## 6.4 Different ratios of the time discretization between the subdomains

Figure 8: Error component estimates evolution with the GMRES solver for different nonconformity ratios of discretization in time N_5/N_i, $i \neq 5$: 10, 5, 2, 1 (from top left to bottom right)

To shed more light on the choice of increased time resolution in the repository domain $\tilde{\Omega}_5$ versus the error induced because of nonconformity of the time grids, we plot in Figure 8 the evolution of our estimates of different error components for different ratios of the time discretization between the central subdomain $\tilde{\Omega}_5$

and the surrounding subdomains $\tilde{\Omega}_i$, $i \neq 5$, namely

$$\frac{N_5}{N_i} = \frac{1000}{100} = 10 \text{ (top left)} , \quad \frac{N_5}{N_i} = \frac{1000}{200} = 5 \text{ (top right; the setting of Section 6.3)},$$

$$\frac{N_5}{N_i} = \frac{400}{200} = 2 \text{ (bottom left)} , \quad \frac{N_5}{N_i} = \frac{250}{250} = 1 \text{ (bottom right; the setting of Section 6.2)}.$$

We can observe that in all cases, the discretization in space estimator (black) remains approximately the same, which confirms numerically that it is indeed given by the discretization error in space. The discretization in time estimator (magenta) 1) goes steeply up when the number of time steps in the central subdomain decreases (between top right and bottom left); 2) is relatively stable when the number of time steps in the other subdomains is changed (between top left and top right); 3) goes up when the overall number of time steps decreases (between bottom left and bottom right). This confirms numerically both that it is connected with the time discretization error and that it is the number of time steps in the central subdomain that is the most important. Finally, the curve for $\eta^k_{\mathrm{DD,NC_{tm}}}$ estimator (green), goes down when the nonconformity-in-time discretization ratio decreases from 10 to 2, but for each ratio it becomes stable after a certain number of iterations. Importantly, when the nonconformity ratio is 1 (bottom right), we come back to the case of a conforming time grid, and, as expected, the green continues to decrease with DD iterations as now no time discretization error is included in this curve, see Remark 7. We can thus conclude that numerically $\eta^k_{\mathrm{DD,NC_{tm}}}$ represents well both the error from the DD iterations and from time-nonconforming grids and that $N_5/N_i = 10$ is the highest reasonable time nonconformity which does not dominate the other error components.

Remark 13 (Test case with known solution). *In [4] we have shown numerical results for the heat equation with known solution $p(x, y, t) = \sin(2\pi x) \sin(2\pi y) \cos(2\pi t)$ and conforming time grids. We have in particular compared the total estimator to an approximation of the error $|||p - \tilde{p}^k_{h\tau}|||_Y$ given by $\{|||p - \tilde{p}^k_{h\tau}|||^2_X + ||(p - \tilde{p}^k_{h\tau})(\cdot, T)||^2\}^{\frac{1}{2}}$ without the term $||\partial_t(p - \tilde{p}^k_{h\tau})||_{X'}$. The evaluation of this term would be rather expensive and we know from [24, Remark 3.3] that one can expect $||\partial_t(p - \tilde{p}^k_{h\tau})||_{X'} \lesssim |||p - \tilde{p}^k_{h\tau}|||_X$. We observed in [4] that the effectivity index in this case approaches the value of approximately 7; importantly, it depends neither on the final time T, nor on the spatial and temporal meshes. Its deviation from to the optimal value of 1 can in part be explained by the fact that the negative norm in $|||p - \tilde{p}^k_{h\tau}|||_Y$ has not been computed.*

References

[1] Y. Achdou, C. Bernardi, and F. Coquel. A priori and a posteriori analysis of finite volume discretizations of Darcy's equations. *Numer. Math.*, 96(1):17–42, 2003.

[2] M. Ainsworth. A posteriori error estimation for lowest order Raviart–Thomas mixed finite elements. *SIAM J. Sci. Comput.*, 30(1):189–204, 2007.

[3] S. Ali Hassan, C. Japhet, M. Kern, and M. Vohralík. A posteriori stopping criteria for optimized Schwarz domain decomposition algorithms in mixed formulations. *Comput. Methods Appl. Math.*, 2018. DOI 10.1515/cmam-2018-0010.

[4] S. Ali Hassan, C. Japhet, M. Kern, and M. Vohralík. Space-time domain decomposition methods and a posteriori error estimates for the heat equation. In C. Dogbe, editor, *Proceedings of VIe Colloque EDP-Normandie - Caen 2017*, pages 65–87. Fédération Normandie Mathématiques, 2018.

[5] T. Arbogast and Z. Chen. On the implementation of mixed methods as nonconforming methods for second-order elliptic problems. *Math. Comp.*, 64(211):943–972, 1995.

[6] M. Arioli. A stopping criterion for the conjugate gradient algorithms in a finite element method framework. *Numer. Math.*, 97(1):1–24, 2004.

[7] M. Arioli and D. Loghin. Stopping criteria for mixed finite element problems. *Electron. Trans. Numer. Anal.*, 29:178–192, 2007/08.

[8] D. N. Arnold and F. Brezzi. Mixed and nonconforming finite element methods: implementation, post-processing and error estimates. *RAIRO Modél. Math. Anal. Numér.*, 19(1):7–32, 1985.

[9] R. Becker, C. Johnson, and R. Rannacher. Adaptive error control for multigrid finite element methods. *Computing*, 55(4):271–288, 1995.

[10] D. Bennequin, M. J. Gander, and L. Halpern. A homographic best approximation problem with application to optimized Schwarz waveform relaxation. *Math. Comp.*, 78(265):185–223, 2009.

[11] P. M. Berthe, C. Japhet, and P. Omnes. Space-Time Domain Decomposition with Finite Volumes for Porous Media Applications. In J. Erhel, M. Gander, L. Halpern, G. Pichot, T. Sassi, and O. Widlund, editors, *Domain decomposition methods in science and engineering XXI*, volume 98 of *Lect. Notes Comput. Sci. Eng.*, pages 483–490. Springer, 2014.

[12] E. Blayo, L. Debreu, and F. Lemarié. Toward an optimized global-in-time Schwarz algorithm for diffusion equations with discontinuous and spatially variable coefficients. Part 1: the constant coefficients case. *ETNA, Kent State University Library*, 40:170–186, 2013.

[13] E. Blayo, L. Halpern, and C. Japhet. Optimized Schwarz waveform relaxation algorithms with nonconforming time discretization for coupling convection-diffusion problems with discontinuous coefficients. In *Domain decomposition methods in science and engineering XVI*, volume 55 of *Lect. Notes Comput. Sci. Eng.*, pages 267–274. Springer, Berlin, 2007.

[14] E. Burman and A. Ern. Continuous interior penalty *hp*-finite element methods for advection and advection-diffusion equations. *Math. Comp.*, 76(259):1119–1140, 2007.

[15] C. Cancès, I. S. Pop, and M. Vohralík. An a posteriori error estimate for vertex-centered finite volume discretizations of immiscible incompressible two-phase flow. *Math. Comp.*, 83(285):153–188, 2014.

[16] P. Ciarlet, E. Jamelot, and F. D. Kpadonou. Domain decomposition methods for the diffusion equation with low-regularity solution. *Comput. Math. Appl.*, 74(10):2369–2384, 2017.

[17] L. C. Cowsar, J. Mandel, and M. F. Wheeler. Balancing domain decomposition for mixed finite elements. *Math. Comp.*, 64(211):989–1015, 1995.

[18] F. Cuvelier. Personal communication. 2016.

[19] F. Cuvelier, C. Japhet, and G. Scarella. An efficient way to assemble finite element matrices in vector languages. *BIT*, 56(3):833–864, 2016.

[20] D. A. Di Pietro, E. Flauraud, M. Vohralík, and S. Yousef. A posteriori error estimates, stopping criteria, and adaptivity for multiphase compositional Darcy flows in porous media. *J. Comput. Phys.*, 276:163–187, 2014.

[21] V. Dolean, P. Jolivet, and F. Nataf. *An introduction to domain decomposition methods*. Society for Industrial and Applied Mathematics (SIAM), Philadelphia, PA, 2015. Algorithms, theory, and parallel implementation.

[22] V. Dolejší, A. Ern, and M. Vohralík. *hp*-adaptation driven by polynomial-degree-robust a posteriori error estimates for elliptic problems. *SIAM J. Sci. Comput.*, 38(5):A3220–A3246, 2016.

[23] J. Douglas, Jr., P. J. Paes-Leme, J. E. Roberts, and J. P. Wang. A parallel iterative procedure applicable to the approximate solution of second order partial differential equations by mixed finite element methods. *Numer. Math.*, 65(1):95–108, 1993.

[24] A. Ern, I. Smears, and M. Vohralík. Guaranteed, locally space-time efficient, and polynomial-degree robust a posteriori error estimates for high-order discretizations of parabolic problems. *SIAM J. Numer. Anal.*, 55(6):2811–2834, 2017.

[25] A. Ern and M. Vohralík. A posteriori error estimation based on potential and flux reconstruction for the heat equation. *SIAM J. Numer. Anal.*, 48(1):198–223, 2010.

[26] A. Ern and M. Vohralík. Adaptive inexact Newton methods with a posteriori stopping criteria for nonlinear diffusion PDEs. *SIAM J. Sci. Comput.*, 35(4):A1761–A1791, 2013.

[27] A. Ern and M. Vohralík. Polynomial-degree-robust a posteriori estimates in a unified setting for conforming, nonconforming, discontinuous Galerkin, and mixed discretizations. *SIAM J. Numer. Anal.*, 53(2):1058–1081, 2015.

[28] C. Farhat and F.-X. Roux. A method of finite element tearing and interconnecting and its parallel solution algorithm. *Internat. J. Numer. Methods Engrg.*, 32(6):1205–1227, 1991.

[29] M. J. Gander. Optimized Schwarz methods. *SIAM J. Numer. Anal.*, 44(2):699–731, 2006.

[30] M. J. Gander, L. Halpern, and M. Kern. A Schwarz waveform relaxation method for advection-diffusion-reaction problems with discontinuous coefficients and non-matching grids. In *Domain decomposition methods in science and engineering XVI*, volume 55 of *Lect. Notes Comput. Sci. Eng.*, pages 283–290. Springer, Berlin, 2007.

[31] M. J. Gander, L. Halpern, and F. Nataf. Optimal Schwarz waveform relaxation for the one dimensional wave equation. *SIAM J. Numer. Anal.*, 41(5):1643–1681, 2003.

[32] M. J. Gander and C. Japhet. Algorithm 932: PANG: software for nonmatching grid projections in 2D and 3D with linear complexity. *ACM Trans. Math. Software*, 40(1):Art. 6, 25, 2013.

[33] M. J. Gander, C. Japhet, Y. Maday, and F. Nataf. A new cement to glue nonconforming grids with Robin interface conditions: the finite element case. In *Domain decomposition methods in science and engineering*, volume 40 of *Lect. Notes Comput. Sci. Eng.*, pages 259–266. Springer, Berlin, 2005.

[34] F. Haeberlein. *Time Space Domain Decomposition Methods for Reactive Transport — Application to CO2 Geological Storage.* Ph.D. thesis, Université Paris-Nord - Paris XIII, 2011.

[35] F. Haeberlein, L. Halpern, and A. Michel. Newton-Schwarz optimised waveform relaxation Krylov accelerators for nonlinear reactive transport. In *Domain decomposition methods in science and engineering XX*, volume 91 of *Lect. Notes Comput. Sci. Eng.*, pages 387–394. Springer, Heidelberg, 2013.

[36] L. Halpern, C. Japhet, and J. Szeftel. Discontinuous Galerkin and nonconforming in time optimized Schwarz waveform relaxation. In *Domain Decomposition Methods in Science and Engineering XIX*, volume 78 of *Lect. Notes Comput. Sci. Eng.*, pages 133–140. Springer, Heidelberg, 2011.

[37] L. Halpern, C. Japhet, and J. Szeftel. Optimized Schwarz waveform relaxation and discontinuous Galerkin time stepping for heterogeneous problems. *SIAM J. Numer. Anal.*, 50(5):2588–2611, 2012.

[38] F. Hecht, O. Pironneau, J. Morice, A. Le Hyaric, and K. Ohtsuka. FreeFem++. Technical report, Laboratoire Jacques-Louis Lions, Université Pierre et Marie Curie, Paris, `http://www.freefem.org/ff++`, 2012.

[39] T.-T.-P. Hoang, J. Jaffré, C. Japhet, M. Kern, and J. E. Roberts. Space-time domain decomposition methods for diffusion problems in mixed formulations. *SIAM J. Numer. Anal.*, 51(6):3532–3559, 2013.

[40] T.-T.-P. Hoang, C. Japhet, M. Kern, and J. E. Roberts. Space-time domain decomposition for reduced fracture models in mixed formulation. *SIAM J. Numer. Anal.*, 54(1):288–316, 2016.

[41] T. T. P. Hoang, C. Japhet, M. Kern, and J. E. Roberts. Space-time domain decomposition for advection-diffusion problems in mixed formulations. *Math. Comput. Simulation*, 137:366–389, 2017.

[42] C. Japhet and F. Nataf. The best interface conditions for domain decomposition methods: absorbing boundary conditions. In *Absorbing Boundaries and Layers, Domain Decomposition Methods*, pages 348–373. Nova Sci. Publ., Huntington, NY, 2001.

[43] P. Jiránek, Z. Strakoš, and M. Vohralík. A posteriori error estimates including algebraic error and stopping criteria for iterative solvers. *SIAM J. Sci. Comput.*, 32(3):1567–1590, 2010.

[44] O. A. Karakashian and F. Pascal. A posteriori error estimates for a discontinuous Galerkin approximation of second-order elliptic problems. *SIAM J. Numer. Anal.*, 41(6):2374–2399, 2003.

[45] K. Y. Kim. A posteriori error analysis for locally conservative mixed methods. *Math. Comp.*, 76(257):43–66, 2007.

[46] P. Ladevèze and J.-P. Pelle. *Mastering calculations in linear and nonlinear mechanics*. Mechanical Engineering Series. Springer-Verlag, New York, 2005. Translated from the 2001 French original by Theofanis Strouboulis.

[47] P.-L. Lions. On the Schwarz alternating method. III: a variant for nonoverlapping subdomains. In R. G. J. P. T. F. Chan and O. Widlund, editors, *Third International Symposium on Domain Decomposition Methods for Partial Differential Equations, held in Houston, Texas, March 20-22, 1989*, pages 202–223. Philadelphia, PA, SIAM, 1990.

[48] J. Mandel. Balancing domain decomposition. *Comm. Numer. Methods Engrg.*, 9(3):233–241, 1993.

[49] V. Martin. An optimized Schwarz waveform relaxation method for the unsteady convection diffusion equation in two dimensions. *Appl. Numer. Math.*, 52(4):401–428, 2005.

[50] D. Meidner, R. Rannacher, and J. Vihharev. Goal-oriented error control of the iterative solution of finite element equations. *J. Numer. Math.*, 17(2):143–172, 2009.

[51] J. Papež, U. Rüde, M. Vohralík, and B. Wohlmuth. Sharp algebraic and total a posteriori error bounds for h and p finite elements via a multilevel approach. HAL Preprint 01662944, 2017.

[52] J. Papež, Z. Strakoš, and M. Vohralík. Estimating and localizing the algebraic and total numerical errors using flux reconstructions. *Numer. Math.*, 138(3):681–721, 2018.

[53] A. T. Patera and E. M. Rønquist. A general output bound result: application to discretization and iteration error estimation and control. *Math. Models Methods Appl. Sci.*, 11(4):685–712, 2001.

[54] G. V. Pencheva, M. Vohralík, M. F. Wheeler, and T. Wildey. Robust a posteriori error control and adaptivity for multiscale, multinumerics, and mortar coupling. *SIAM J. Numer. Anal.*, 51(1):526–554, 2013.

[55] W. Prager and J. L. Synge. Approximations in elasticity based on the concept of function space. *Quart. Appl. Math.*, 5:241–269, 1947.

[56] S. Repin. *A posteriori estimates for partial differential equations*, volume 4 of *Radon Series on Computational and Applied Mathematics*. Walter de Gruyter GmbH & Co. KG, Berlin, 2008.

[57] V. Rey, P. Gosselet, and C. Rey. Strict bounding of quantities of interest in computations based on domain decomposition. *Comput. Methods Appl. Mech. Engrg.*, 287:212–228, 2015.

[58] V. Rey, P. Gosselet, and C. Rey. Strict lower bounds with separation of sources of error in non-overlapping domain decomposition methods. *Internat. J. Numer. Methods Engrg.*, 108(9):1007–1029, 2016.

[59] V. Rey, C. Rey, and P. Gosselet. A strict error bound with separated contributions of the discretization and of the iterative solver in non-overlapping domain decomposition methods. *Comput. Methods Appl. Mech. Engrg.*, 270:293–303, 2014.

[60] V. Thomee. *Galerkin Finite Element Methods for Parabolic Problems*. Springer, 1997.

[61] R. Verfürth. A posteriori error estimates for finite element discretizations of the heat equation. *Calcolo*, 40(3):195–212, 2003.

[62] M. Vohralík. A posteriori error estimates for lowest-order mixed finite element discretizations of convection-diffusion-reaction equations. *SIAM J. Numer. Anal.*, 45(4):1570–1599, 2007.

[63] M. Vohralík. Unified primal formulation-based a priori and a posteriori error analysis of mixed finite element methods. *Math. Comp.*, 79(272):2001–2032, 2010.